Fabrication of transparent Ce^{3+}-doped $(Gd,Lu)_3Al_5O_{12}$ ceramics by two-step spark plasma sintering

Ji-Hwoan Lee[a], Byung-Nam Kim[a], Ji-Guang Li[a], and Byung-Koog Jang[b,*]

[a] Research Center for Functional Materials, National Institute for Materials Science, 1-2-1 Sengen, Tsukuba, Ibaraki 305-0047, Japan

[b] Interdisciplinary Graduate School of Engineering Science, Kyushu University, 6-1 Kasuga-koen, Kasuga, Fukuoka 816-8580, Japan

*Corresponding author:

E-mail address: jang.byungkoog@kyudai.jp (B.K. Jang)

Abstract

Transparent Ce^{3+}:$(Gd,Lu)_3Al_5O_{12}$ with microstructure control were fabricated by two-step spark plasma sintering. In the two-step profile, the heating rate was changed from 50 to 5°C/min at the first-step temperatures. During the initial stage of shrinkage, the holding time of the first-step sintering could induce densification by suppressing the microstructure coarsening. As compared to the single-step profile, the two-step profile showed smaller grain size, which decreased with a decrease in the first-step temperature. The porosity of the two-step profile was lower than that of the single-step profile, and the lowest porosity was obtained at the first-step temperature of 1000°C, which was the starting point of shrinkage. The TS-1000 specimen showed the highest transmittance among all the specimens because of the microstructure control offered by the two-step profile. Thus, by employing the two-step profile, the transmittance could be increased from 50.1% (SS-1250) to 56.5% (TS-1000).

Keywords: Two-step spark plasma sintering; Optical property; Photoluminescence characteristics; Microstructure; Gadolinium and lutetium aluminum garnet

1. Introduction

Lanthanide aluminum garnets ($Ln_3Al_5O_{12}$, LnAG), represented by $Gd_3Al_5O_{12}$ (GdAG) and $Lu_3Al_5O_{12}$ (LuAG), have high theoretical densities, and are attractive candidates for scintillator applications. LnAGs exhibit unique properties, such as wide bandgaps, high chemical and thermal stability, and wide transparent range, which make them suitable for scintillator applications [1–4]. Scintillators should possess high theoretical density to stop X-rays. YAG shows relatively X-ray low stopping power owing to its low density (4.53 g/cm^3). Among the lanthanide elements with atomic weights higher than Y (89), Gd (157), and Lu (174) are considered as suitable candidates for increasing the density of the garnet structure. However, Gd (0.21 ppm) and Lu (0.02 ppm) are less abundant in the earth's crust as compared to Y (1.39 ppm) [5]. As Gd is more abundant than Lu, it is considered as a more suitable substitute for Y. Recently, transparent Gd-based LnAGs have been extensively investigated for scintillator applications. However, GdAGs thermally decompose into $GdAlO_3$ perovskite and Al_2O_3 above 1300°C ($Gd_3Al_5O_{12} \rightarrow 3GdAlO_3 + Al_2O_3$) [6]. In addition, GdAGs are doped with Ce^{3+} as an activator of yellow-emitting phosphors. The larger Ce^{3+} ions cause the destabilization of the garnet structure, thereby reducing its thermal decomposition temperature. In order to suppress their thermal decomposition, Ce-doped GdAGs are doped with Lu^{3+} ions, which are much smaller than Gd^{3+} ions [7]. These Lu^{3+} ions reduce the average Ln^{3+} size, and hence stabilize the garnet structure. In addition, Lu^{3+} doping retains the photoluminescence (PL) characteristics of Ce^{3+} and increases the theoretical density of Ce^{3+}:$(Gd,Lu)_3Al_5O_{12}$, thus enabling the development of advanced yellow-emitting phosphors [7].

Decreasing the sintering temperature can prevent the thermal decomposition of GdAG above 1300°C and improve its mechanical properties while providing a dense microstructure.

Among the various sintering techniques, spark plasma sintering (SPS) controlled by an electric field and mechanical pressure is considered as an efficient sintering approach for GdAG [8,9]. In the SPS process, the electric field rapidly heats the mold and powder compact, facilitating the rapid densification by several microscopic mechanisms, including increased atom diffusivity and softening of the particle surfaces, so that excessive grain growth is suppressed at low temperatures [8,10]. Therefore, high densities and fine microstructures, which are the advantages of SPS, improve the mechanical and optical properties of ceramics. Recently, the fabrication and characterization of LuAG ceramics, such as Nd:YAG [11], LuAG [12], and Ce^{3+}:$(Gd,Lu)_3Al_5O_{12}$ [13], using the SPS process have been reported [11–13]. Sufficient transparency can be obtained by conventional sintering, hot pressing (HP), and hot isostatic pressing (HIP) [14–16]. However, the fabrication of transparent LnAG using the SPS process has not been sufficiently studied. In our previous work [13], a Ce^{3+}:$(Gd,Lu)_3Al_5O_{12}$ powder was fully densified using the SPS process, but a transparent compact was not obtained. Therefore, further research is required to improve the transparency of SPS-prepared ceramics while retaining the intrinsic merits of the SPS technique.

Various studies have reported the application of a two-step sintering profile to the conventional sintering, HP, and HIP techniques to improve the optical properties and control the microstructure of ceramics [16–19]. Previous studies on the two-step sintering profile suggested that preliminary experiments on microstructure control should be conducted to improve the optical properties of ceramics [18,19]. Although the two-step sintering profile is applied in different ways, the main objective is to achieve primary densification without excessive coarsening at the higher first-step temperature and full densification and removal of residual pores during the second step sintering. As a result, full densification can be effectively

achieved by dividing the sintering process into two steps with different objectives. In addition, some researchers have reported that a two-step profile can be applied to improve the optical properties of ceramics while retaining the intrinsic merits of the SPS process [20–24]. In the SPS process, the two-step profile is applied in a slightly different way, because the amount of carbon contamination and residual pores inevitably increases with an increase in the sintering time. Considerable research [22,23] has been carried out on the microstructure and optical properties of each step of the two-step profile. After primary densification without excessive microstructure coarsening when the first step temperature is lower than the second step temperature, sufficient densification and excellent transparency could be achieved by removing the residual defects at the second-step temperature. In our previous work [24], in transparent Y_2O_3 fabricated with a lower first-step temperature, microstructural control and improved optical properties could be achieved. On the basis of the previously reported results on the two-step profile, it can be stated that by suppressing excessive microstructure coarsening and separating the primary densification and full densification processes, the microstructure of LnAG can be made fine and dense and its transmittance can be improved.

In this study, a two-step SPS profile was employed to improve the optical properties of transparent Ce^{3+}:$(Gd,Lu)_3Al_5O_{12}$ ceramics while controlling their microstructure. The two-step profile involved first-step sintering at 900, 1000, and 1200°C and second-step sintering at 1250°C. The first-step sintering provided primary densification and suppressed excessive microstructure coarsening. The second-step sintering on the other hand, provided full densification and the removal of the residual pores along with microstructure control. The microstructure and optical properties of the ceramics were evaluated by focusing on the microstructure control by varying the first-step temperature.

2. Experimental Procedure

2.1. Preparation of Ce^{3+}:$(Gd,Lu)_3Al_5O_{12}$ powder

The rare-earth and aluminum sources used in this study were Ln_2O_3 (Ln = Gd and Lu, 99.99%, Huizhou RUIER Rare-Chem. Hi-Tech, China), $Ce(NO_3)_3 \cdot 6H_2O$ (99.99%, Huizhou Ruier Rare-Chem. Hi-Tech, China), and alum ($NH_4Al(SO_4)_2 \cdot 12H_2O$, > 99%, Zhenxin Chemical Reagent Factory, China). A $Ln(NO_3)_3$ stock solution was prepared by dissolving the oxide powders in an optimum amount of nitric acid. To precipitate the carbonate precursor, a mixed solution containing the stoichiometric amounts of the nitrates and alum was added dropwise to the ammonium bicarbonate solution. The precipitated carbonate precursor was dried in an oven for 24 h. The $[(Gd_{0.6}Lu_{0.4})_{0.99}Ce_{0.01}]_3Al_5O_{12}$ powder was obtained by the thermal decomposition of the precursor *via* calcination at 1100°C for 4 h in air. To suppress the oxidation of Ce^{3+}, a second calcination process was performed at 1000°C for 4 h in Ar/H_2 (5 vol% of H_2) [7,25].

2.2. Consolidation of Ce^{3+}:$(Gd,Lu)_3Al_5O_{12}$ compacts using SPS process

The Ce^{3+}:$(Gd,Lu)_3Al_5O_{12}$ powder was consolidated using SPS equipment (LABOX-315, Sinter Land, Japan) under a vacuum atmosphere of 10 Pa. The powder was directly sintered without any pre-treatment, using a graphite mold with a diameter of 10 mm. Heating was performed using a pulse pattern of 5:5 (on:off) in the AC mode, and temperature was measured by installing a pyrometer in the non-through hole of the mold. The entire SPS process was divided into single-step and two-step profiles. For the single-step profile, the powder compact was heated to a sintering temperature of 1250°C at a heating rate of 50°C/min, and held for 20 min. In the case of the two-step profile, to achieve primary densification without excessive microstructure coarsening, the first-step sintering was performed at 900, 1000, and 1200°C with

heating rate of 50°C/min and the sintering temperature was held for 30 min. In the single-step profile, shrinkage started at approximately 1000°C. Thus, the first-step temperature for the two-step profile was considered to be 1000°C. To achieve full densification and the removal of the residual pores, further heating was conducted to reach the second-step temperature of 1250°C at 5°C/min. This temperature was held for 20 min. In the entire SPS process, a mechanical pressure of 6.5 kN (80 MPa) was applied from the beginning and was maintained until before cooling. In addition, cooling was sequentially performed at 1100°C for 10 min, 800°C for 5 min, and 25°C for 5 min. The SPS conditions and specimen names are listed in Table 1.

2.3. Characterization

The annealing process was conducted at 1250°C for 10 h in air to remove the carbon contamination and oxygen vacancies. Both the surfaces of the Ce^{3+}:$(Gd,Lu)_3Al_5O_{12}$ compacts were mirror polished with 9, 3, and 1 μm diamond pastes. The transmittance of the compacts was measured using a double-beam spectrophotometer (SolidSpec-3700DUV, Shimazu, Japan) equipped with an integrating sphere. PL measurements were conducted using a spectrofluorometer (FP-6500, JASCO, Japan) equipped with a 60 mm diameter-integrating sphere (Model ISF-513, JASCO, Japan) and a 150 W Xe lamp as the excitation source. The X-ray photoelectron spectroscopy (XPS, AXIS-165, Shimadzu, Japan) profiles of the samples were recorded at room temperature with Al-K_α radiation for excitation. The binding energy was referenced to the C-1 s line of adventitious carbon. The mirror-polished surfaces were thermally etched at 1100°C for 2 h in air. The polished and fracture surfaces of the specimens were examined using scanning electron microscopy (SEM, SU-8000, Hitachi, Japan). The porosity of the specimens was determined by measuring their porous areas from the SEM images. The

grain and pore sizes of the specimens were calculated by measuring their average cross-sectional areas per grain and pore sizes. The grain size was apparent in the cross-section; therefore, it was multiplied by 1.225 to determine the actual grain size [26].

3. Results and Discussion

3.1. Shrinkage behavior and microstructure

In our previous work, we successfully developed a stable $(Gd,Lu)_3Al_5O_{12}$ garnet structure, which could be well indexed to the cubic structure of GdAG [13]. Single-step and two-step SPS profiles were applied to fabricate transparent $(Gd,Lu)_3Al_5O_{12}$ ceramics with structural stabilization. The SPS curves (temperature, displacement, and pressure over time) of the single-step profile (SS-1250) are shown in Fig. 1 (a). As can be observed from the displacement curve, the ceramics showed thermal expansion when heated to approximately 1000°C. In addition, shrinkage began to occur at this temperature. No further shrinkage occurred during the holding period at 1250°C, and the shrinkage was sufficient. Based on the SPS curves of the single-step profile (SS-1250), a two-step profile (TS-1000) was designed, as shown in Fig. 1 (b). At a relatively low first-step temperature of 1000°C, the powder compact was rapidly heated at 50°C/min to suppress excessive microstructure coarsening, and primary densification was performed for 30 min [20,22,24]. In addition, during the first-step holding time, as the shrinkage began and did not occur rapidly, a small amount of the residual pores could be expected. Owing to the achievement of the primary densification, including a small amount of the residual pores in the first-step sintering, the shrinkage of the two-step profile was completed at 1200°C, which is approximately 50°C lower than that 1250°C of the single-step profile, although the amount of shrinkage was almost the same. This improvement in the sintering behavior of the compacts by the two-step profile not only enabled microstructure control but can also improve the optical properties.

Fig. 2 shows the SEM images of the cross-sections of the SPSed Ce^{3+}:$(Gd,Lu)_3Al_5O_{12}$ compacts after annealing. All the specimens densified at the final sintering temperature of

1250°C. However, the microstructures for the two SPS profile differed in terms of the grain size, pore size, and porosity. The microstructural parameters (grain size, pore size, and porosity) calculated from the SEM images are summarized in Table 2. By applying the two-step profile, it was possible to significantly lower the porosity at the same sintering temperature. All the two-step SPSed specimens showed lower porosity than the single-step SPSed specimen (SS-1250) (3.74%). In particular, TS-1000 exhibited a porosity of 1.63%, indicating that significant reduction in the porosity was possible by applying the two-step SPS profile. A significant decrease in the porosity of the two-step SPSed specimens was due to the improvement in their shrinkage behavior, i.e., the smaller amount of residual pores and the lower shrinkage completion temperature, as shown in Fig. 2. In addition, as the first-step temperature in the two-step profile was reduced, the grain size decreased gradually from 207 to 139 nm, and the pore size decreased from 72 to 43 nm. This microstructural change was due to the microstructure control of the two-step profile [18,19]. In this study, the microstructure control using the two-step profile was expected to improve the optical properties as well.

3.2. Optical appearance and transmittance

The optical appearances of the Ce^{3+}:$(Gd,Lu)_3Al_5O_{12}$ compacts after annealing are shown in Fig. 3. The optical appearances and transparency of the annealed specimens placed on the grid can be easily compared. SS-1250 exhibited the lowest optical transparency among all the specimens. The application of the modified two-step profile improved the optical appearance of the compacts. For the two-step SPSed specimens, the optical appearance improved with a decrease in the heating rate at second-step. However, the most significant improvement was observed at the first-step temperature of 1000°C. This indicates that a decrease in the heating

rate at the critical temperature for densification had more significant effect than simply reducing the heating rate to improve the optical appearance. Therefore, at the first-step temperature of 1000°C, the porosity was the lowest and the optical appearance also improved the most. The microstructure and optical appearance analysis results indicate that the TS-1000 specimen showed the highest transmittance among all the specimens investigated in this study.

Fig. 4 shows the in-line transmittance (ILT) curves of the sintered Ce^{3+}:$(Gd,Lu)_3Al_5O_{12}$ compacts after annealing. Significant light absorption was in the range of 420–500 nm. Owing to the light absorption due to the $4f \rightarrow 5d_2$ and $4f \rightarrow 5d_1$ transitions of Ce^{3+} at 340 nm and over the wavelength range of 420–500 nm, respectively, strong absorption occurred at thesis wavelengths [27]. The optical transmittance of the specimens showed the same trend as that shown by their optical appearance. At the same sintering temperature of 1250°C, all the two-step SPSed specimens showed improved transmittance as compared to the single-step SPSed specimen. The TS-1000 specimen showed the most improved ILT of 56.5% at 1000 nm as compared to that (50.1%) of the SS-1250 specimen. In transparent ceramics, the area of the grain boundary also affects the transmittance; however, the porosity is the most critical factor [28]. In the case of the TS-1000 specimen, the first-step temperature was 1000°C, at which the shrinkage began, and the porosity decreased significantly from 3.74% (SS-1250) to 1.63% (TS-1000). This decrease in the porosity had a significant effect on the transmittance of the ceramic. In addition, as can be observed from Table 2, the porosity of the specimens showed a trend similar to that shown by the optical transmittance. The TS-1000 specimen showed slightly reduced grain and pore sizes and significantly reduced porosity as compared to the SS-1250 specimen. The decrease in the porosity, which had the most critical effect on the transmittance, resulted in the most noticeable improvement in the transmittance of the TS-1000 specimen.

$(Gd,Lu)_3Al_5O_{12}$:Ce ceramics with a composition similar to that of the ceramics prepared in this study were fabricated by conventional sintering at 1750°C for 4 h under a vacuum atmosphere after cold isostatic press at 240 MPa [14]. As a result, an ILT of approximately 72% was achieved at 1000 nm, showing excellent optical properties. Although there have been reports of preparing garnet materials with full densification and high transmittance by conventional sintering, it is difficult to achieve high transmittance with the SPS method. Ina a previous study, Nd:YAG ceramics were fabricated using the reactive-SPS method by applying a two-step heating profile [29]. The Nd:YAG powder was heated at 100°C/min to the first-step temperature of 1000°C with an applied pressure of 70 MPa and at 15°C/min to the second-step temperature of 1350°C, which was maintained for 5 min. However, an ILT of approximately 36% was obtained at 1000 nm, and excellent optical properties were not achieved. In this study, although the ILT was not close to the theoretical value, the transmittance could be improved through the application of the two-step profile and microstructure control.

3.3. Oxidation state and PL characteristic

XPS measurements were conducted to investigate the oxidation states of the Ce dopant, and the results of the powder, single-step profile (SS-1250), and two-step profile (TS-1000) are summarized in Fig. 5. The red lines represent the spectra of Ce^{3+} ions and the blue lines represents the spectra of Ce^{4+} ions. The fractions of the Ce^{3+} and Ce^{4+} ions were calculated from the areas of their spectra. For comparing the as-synthesized powder with the compacts sintered in the single-step and two-step profiles, the fraction of Ce^{3+} in the as-synthesized powder was required. The fraction of Ce^{3+} in the powder was 61.42%, as shown in Fig. 5 (a). The Ce^{3+} fraction of the SS-1250 specimen was 61.73%, which is almost the same as that of the

synthesized powder. However, the TS-1000 specimen showed a Ce^{3+} fraction of 60.66% because of slight oxidation. As the SPS process provides an oxidizing atmosphere of graphite components, oxidation occurred in the two-step profile with a long sintering time, and the fraction of Ce^{3+} decreased slightly. The slightly decreased Ce^{3+} fraction of the two-step profile affected its PL characteristics along with the microstructure.

Fig. 6 (a) shows the PL excitation spectra of the Ce^{3+}:$(Gd,Lu)_3Al_5O_{12}$ compacts after annealing. PL excitation measurements were performed to investigate the wavelength-dependent excitation when 571 nm light was emitted. Excitation bands were detected at approximately 342, 453, and 506 nm, which correspond to the excitation of Ce^{3+} [30,31]. The excitation peak at approximately 342 nm corresponded to the transition of Ce^{3+} from the ground state ($2F_{5/2}$) to the T_{2g} state. The excitation peaks at approximately 453 and 506 nm corresponded to the transition from the ground state to the E_{2g} state [30,31]. The SS-1250 specimen exhibited significantly higher PL excitation intensity than the two-step profile specimens. Independent of the first-step temperature, the PL excitation of the TS-1000 specimen intensity was the lowest. The transmittance of the specimens was strongly influenced by their porosity, and the two-step profile showed better results than the single-step profile. However, the PL excitation characteristics showed an opposite trend. First, the fraction of Ce^{3+} (Fig. 5) directly affected the PL excitation characteristics of the specimens. Because the PL excitation was caused only by Ce^{3+} [30,31], the fraction of Ce^{3+} present in the Ce^{3+}:$(Gd,Lu)_3Al_5O_{12}$ ceramics was a very important factor. Next, the grain size of the SS-1250 specimen was the largest at 221 nm, which decreased gradually from 207 to 139 nm with a decrease in the first-step temperature. Owing to its large grain size and small grain boundary area, the single-step profile affected the PL excitation characteristics of the compacts more than the two-step profile

[32,33]. Fig. 6 (b) shows the PL emission spectra of the Ce^{3+}:$(Gd,Lu)_3Al_5O_{12}$ compacts after annealing. The wavelength-dependent emission of the compacts under excitation by a wavelength of 453 nm was investigated. The PL emission characteristics of the compacts showed the same trend as that shown by the PL excitation characteristics. The full width at half maximum values were almost the same for all the specimens. This indicates that the crystallinity and light clarity of all the specimens were almost the same and that the two-step profile did not affect the PL emission characteristics.

4. Conclusions

In this study, a two-step SPS profile was employed to improve the optical properties of Ce^{3+}:$(Gd,Lu)_3Al_5O_{12}$ ceramics as attractive yellow-emitting phosphors. The shrinkage curve of the two-step profile showed a significant reduction in the porosity from 3.74% to 1.63% at the first-step temperature of 1000°C, at which the shrinkage began. As the first-step temperature decreased, the microstructure control of two-step profile refined the microstructure of the compacts by reducing the grain and pore sizes. As a result of the significant reduction in the porosity in the two-step profile, the transmittance improved from 50.1% to 56.5% at 1000 nm. On the other hand, owing to the long sintering time of the two-step profile, oxidation occurred and the fraction of Ce^{3+} decreased slightly. Therefore, the two-step profile did not affect the PL excitation and emission characteristics of the ceramics.

References

[1] J.G. Li, Y. Sakka, Recent progress in advanced optical materials based on gadolinium aluminate garnet ($Gd_3Al_5O_{12}$), Sci. Technol. Adv. Mater. 16 (2015) 014902.

[2] M. Wang, B. Lu, Manufacture and Faraday magneto-optical effect of highly transparent novel holmium aluminum garnet ceramics, Scripta Mater. 195 (2021) 133729.

[3] I. Milisavljevic, G. Zhang, Y. Wu, Solid-state single-crystal growth of YAG and Nd: YAG by spark plasma sintering, J. Mater. Sci. Technol. 106 (2022) 118–127.

[4] C. Kim, W. Lee, A. Melis, A. Elmughrabi, K. Lee, C. Park, J.Y. Yeom, A Review of Inorganic Scintillation Crystals for Extreme Environments, Crystals 11 (2021) 669.

[5] V. Balaram, Rare earth elements: A review of applications, occurrence, exploration, analysis, recycling, and environmental impact, Geosci. Front. 10 (2019) 1285–1303.

[6] T. Shishido, K. Okamura, S. Yajima, $Gd_3Al_5O_{12}$ Phase Obtained by Crystallization of Amorphous $Gd_2O_3 \cdot 5/3Al_2O_3$, J. Am. Ceram. Soc. 61 (1978) 373–375.

[7] J. Li, J.G. Li, S. Liu, X. Li, X. Sun, Y. Sakka, The development of Ce^{3+}-activated $(Gd,Lu)_3Al_5O_{12}$ garnet solid solutions as efficient yellow-emitting phosphors, Sci. Technol. Adv. Mater. 14 (2013) 054201.

[8] B.N. Kim, K. Morita, T.S. Suzuki, J.G. Li, H. Matsubara, Simulation of densification behavior of nano-powder in final sintering stage: Effect of pore-size distribution, J. Eur. Ceram. Soc. 41 (2021) 625–634.

[9] M. Tokita, Progress of Spark Plasma Sintering (SPS) Method, Systems, Ceramics Applications and Industrialization, Ceramics 4 (2021) 160–198.

[10] A. Wagner, Y. Meshorer, B. Ratzker, D. Sinefeld, S. Kalabukhov, S. Goldring, E. Galun, N. Frage, Pressure‐assisted sintering and characterization of Nd:YAG ceramic lasers, Sci.

Rep. 11 (2021) 1512.

[11] A. Wagner, B. Ratzker, S. Kalabukhov, S. Kolusheva, M. Sokol, N. Frage, Highly-doped Nd:YAG ceramics fabricated by conventional and high pressure SPS, Ceram. Int. 45 (2019) 12279–12284.

[12] S.F. Wang, J. Zhang, D.W. Luo, F. Gu, D.Y. Tang, Z.L. Dong, G.E.B. Tan, W.X. Que, T.S. Zhang, S. Li, L.B. Kong, Transparent ceramics: Processing, materials and applications, Prog. Solid. State. Chem. 41 (2013) 20–54.

[13] J.H. Lee, J.G. Li, B.N. Kim, Q. Meng, X. Sun, B.K. Jang, Effect of annealing on microstructure and luminescence characteristics in spark plasma sintered Ce^{3+}-activated $(Gd,Lu)_3Al_5O_{12}$ garnet ceramics, J. Eur. Ceram. Soc. 41 (2021) 1586–1592.

[14] Z. Sun, Z. Chen, M. Wang, B. Lu, Production and optical properties of Ce^{3+}-activated and Lu^{3+}-stabilized transparent gadolinium aluminate garnet ceramics, J. Am. Ceram. Soc. 103 (2020) 809–818.

[15] X. Chen, X. Liu, Y. Feng, X. Li, H. Chen, T. Xie, H. Kou, R. Kucerkova, Microstructure evolution in two-step-sintering process towardtransparent $Ce:(Y,Gd)_3(Ga,Al)_5O_{12}$ scintillation ceramics. J Alloys Compd. 2020;846;156377.

[16] J. Li, Q. Chen, G. Feng, W. Wu, D. Xiao, J. Zhu, Optical properties of the polycrystalline transparent Nd:YAG ceramics prepared by two-step sintering, Ceram. Int. 38S (2012) S649–S652.

[17] Z. Seeley, N. Cherepy, S. Payne, Two-step sintering of $Gd_{0.3}Lu_{1.6}Eu_{0.1}O_3$ transparent ceramic scintillator, Opt. Mater. Express. 3 (2013) 908–912.

[18] W.K. Jung, H.J. Ma, D.G. Kim, D.K. Kim, Two-step sintering behavior of titanium-doped Y_2O_3 ceramics with monodispersed sub-micrometer powder, Ceram. Int. 45 (2019) 510–

515.

[19] H.J. Ma, W.K. Jung, C. Baek, D.K. Kim, Influence of microstructure control on optical and mechanical properties of infrared transparent Y_2O_3-MgO nanocomposite, J. Eur. Ceram. Soc. 37 (2017) 4902–4911.

[20] H. Furuse, S. Nakasawa, H. Yoshida, K. Morita, T.S. Suzuki, B.N. Kim, Y. Sakka, K. Hiraga, Transparent ultrafine Yb^{3+}:Y_2O_3 laser ceramics fabricated by spark plasma sintering, J. Am. Ceram. Soc. 101 (2018) 694–702.

[21] K. Morita, B.N. Kim, H. Yoshida, H. Zhang, K. Hiraga, Y. Sakka, Effect of loading schedule on densification of $MgAl_2O_4$ spinel during spark plasma sintering (SPS) processing, J. Eur. Ceram. Soc. 32 (2012) 2303–2309.

[22] M. Nanko, K.Q. Dan, Two-step pulsed electric current sintering of transparent Al_2O_3 ceramics, Adv. Appl. Ceram. 113 (2014) 80–84.

[23] H.H. Nguye, M. Nanko, Densification and grain growth of large-sized polycrystalline Al_2O_3 during a two-step pulsed electric current sintering process, Mater. Trans. 59 (2018) 1610–1615.

[24] J.H. Lee, B.N. Kim, B.K. Jang, Fabrication of transparent Y_2O_3 ceramics by two-step spark plasma sintering, J. Am. Ceram. Soc. 104 (2021) 5501–5508.

[25] J. Li, J.G. Li, X. Li, X. Sun, Photoluminescence properties of phosphors based on Lu^{3+}-stabilized $Gd_3Al_5O_{12}$:Tb^{3+}/Ce^{3+} garnet solid solutions, Opt. Mater. 62 (2016) 328–334.

[26] S. Grasso, C. Hu, G. Maizza, B.N. Kim, Y. Sakka, Effects of pressure application method on transparency of spark plasma sintered alumina, J. Am. Ceram. Soc. 94 (2011) 1405–1409.

[27] S. Feng, H. Qin, G. Wu, H. Jiang, J. Zhao, Y. Liu, Z. Luo, J. Qioa, J. Jiang, Spectrum

regulation of YAG:Ce transparent ceramics with Pr, Cr doping for white light emitting diodes application, J. Eur. Ceram. Soc. 37 (2017) 3403–3409.

[28] T. Benitez, S.Y. Gomez, A. Oliveira, N. Travitzky, D. Hotza, Transparent ceramic and glass-ceramic materials for armor applications, Ceram. Int. 43 (2017) 13031–13046.

[29] D.Y. Kosyanov, A.A. Vornovskikh, A.M. Zakharenko, E.A. Gridasova, R.P. Yavetskiy, M.V. Dobrotvorskaya, A.V. Tolmachev, O.O. Shichalin, E.K. Papynov, A.Y. Ustinov, V.G. Kuryavyi, A.A. Leonov, S.A. Tikhonov, Influence of sintering parameters on transparency of reactive SPSed Nd^{3+}:YAG ceramics, Opt. Mater. 112 (2021) 110760.

[30] X. Su, K. Zhang, Q. Liu, H. Zhong, Y. Shi, Y. Pan, Combinatorial Optimization of $(Lu_{1-x}Gd_x)_3Al_5O_{12}:Ce_{3y}$ Yellow Phosphors as Precursors for Ceramic Scintillators, ACS Comb. Sci. 13 (2011) 79–83.

[31] A. Birkel, K.A. Denault, N.C. George, C.E. Doll, B. Hery, A.A. Mikhailovsky, C.S. Birkel, B.C. Hong, R. Seshadri, Rapid Microwave Preparation of Highly Efficient Ce^{3+}-Substituted Garnet Phosphors for Solid State White Lighting, Chem. Mater. 24 (2012) 1198–1204.

[32] B. Wen, D.F. Zhang, N. Zhang, J.K. Feng, B. Jiang, F.S. Pan, Y. Zhang, L. Yang, Effect of grain size on the luminescent properties of Ce^{3+} doped $Y_3Al_5O_{12}$ ceramic phosphor plates, Ceram. Int. 46 (2020) 10452–10456.

[33] Y. Kim, S. Jang, Effect of particle size on photoluminescence emission intensity of ZnO, Acta Mater. 59 (2011) 3024–3031.

Figure captions

Figure 1. Fig. 1. SPS curves of the SPSed Ce^{3+}:$(Gd,Lu)_3Al_5O_{12}$ ceramics (a) single-step SPS (SS-1250) and (b) two-step SPS (TS-1000).

Figure 2. SEM images of the cross-sections of the SPSed Ce^{3+}:$(Gd,Lu)_3Al_5O_{12}$ ceramics.

Figure 3. Optical appearances of the SPSed Ce^{3+}:$(Gd,Lu)_3Al_5O_{12}$ ceramics under the conditions listed in Table 1.

Figure 4. (a) Transmittance curves of the SPSed Ce^{3+}:$(Gd,Lu)_3Al_5O_{12}$ ceramics after annealing. (b) is the curve magnified over the wavelength of 750–1050 nm.

Figure 5. XPS profiles of the (a) Ce^{3+}:$(Gd,Lu)_3Al_5O_{12}$ powder, (b) single-step SPSed compact (SS-1250), and (c) two-step SPSed Compact (TS-1000).

Figure 6. (a) PL excitation and (b) PL emission spectra of the Ce^{3+}:$(Gd,Lu)_3Al_5O_{12}$ ceramics with different SPS conditions after annealing.

Figures

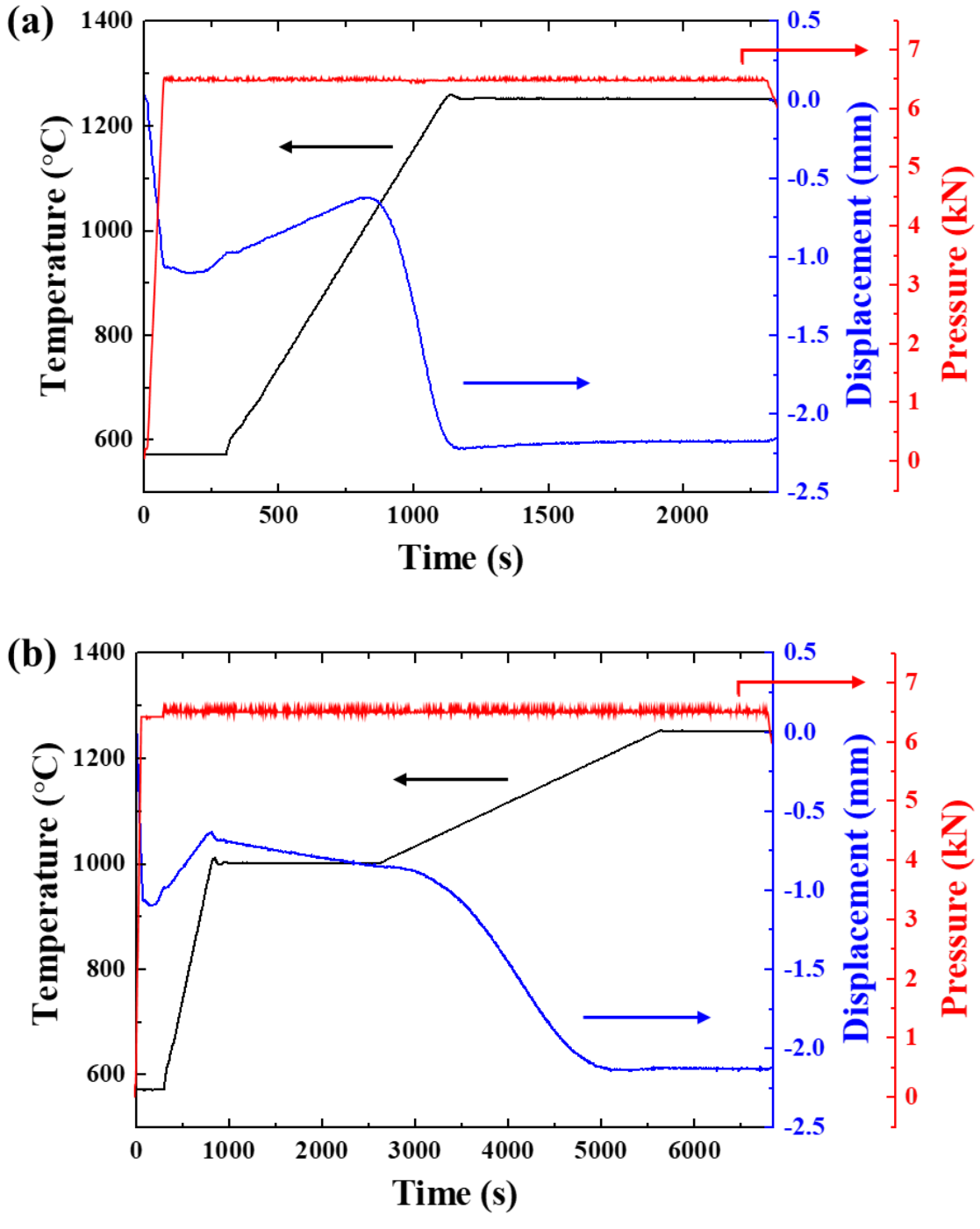

Fig. 1

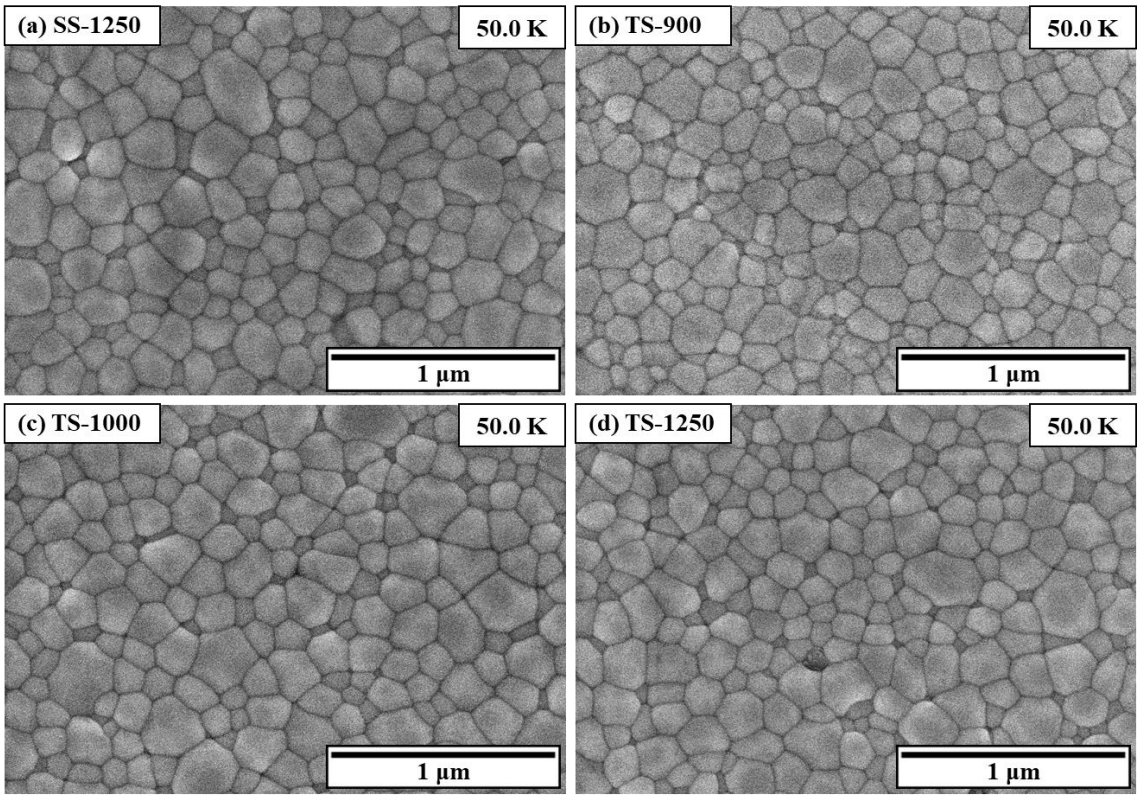
(a) SS-1250
50.0 K
1 µm
(b) TS-900
50.0 K
1 µm
(c) TS-1000
50.0 K
1 µm
(d) TS-1250
50.0 K
1 µm

Fig. 2

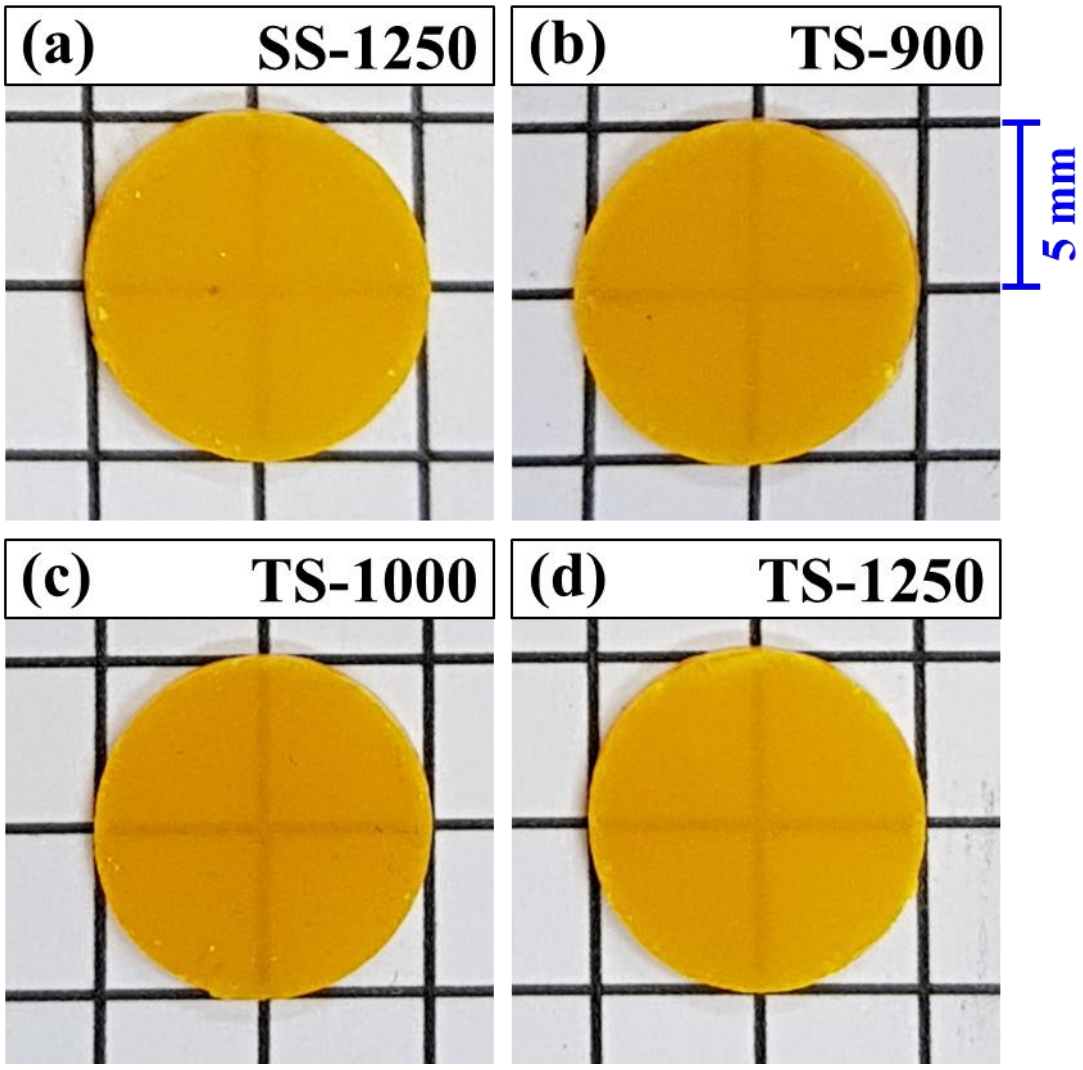

Fig. 3

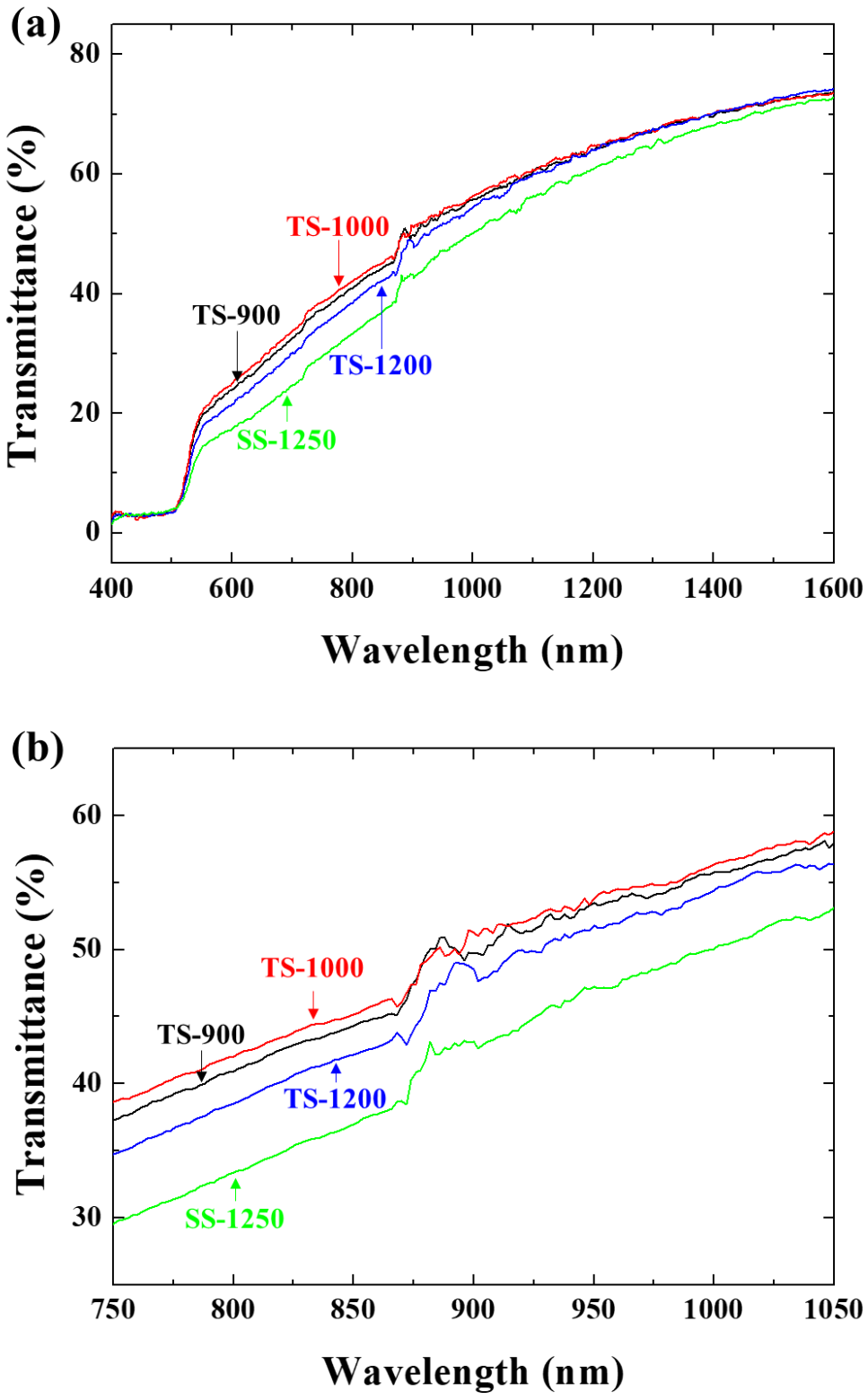
(a)
Transmittance (%)
Wavelength (nm)
TS-900
TS-1000
TS-1200
SS-1250
(b)
Transmittance (%)
Wavelength (nm)
TS-900
TS-1000
TS-1200
SS-1250

Fig. 4

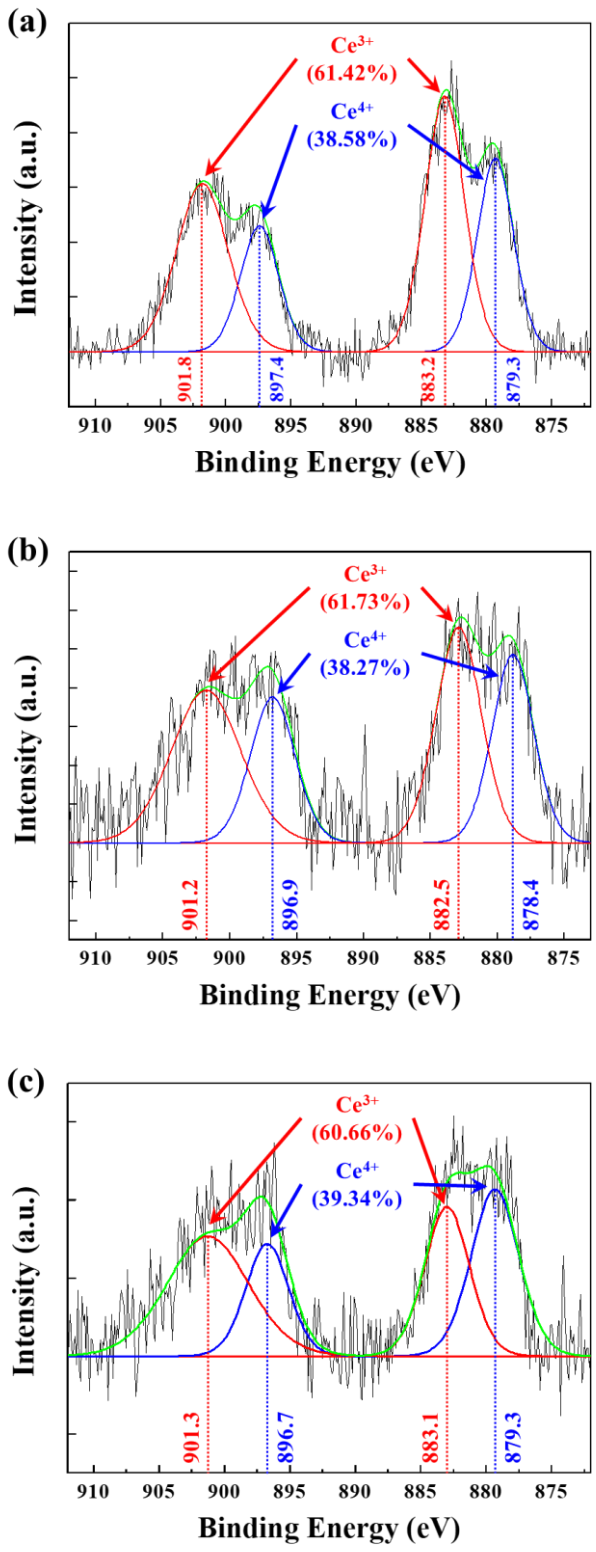
(a)
Ce3+
(61.42%)
Ce4+
(38.58%)
Intensity (a.u.)
901.8
897.4
883.2
879.3
910 905 900 895 890 885 880 875
Binding Energy (eV)
(b)
Ce3+
(61.73%)
Ce4+
(38.27%)
Intensity (a.u.)
901.2
896.9
882.5
878.4
910 905 900 895 890 885 880 875
Binding Energy (eV)
(c)
Ce3+
(60.66%)
Ce4+
(39.34%)
Intensity (a.u.)
901.3
896.7
883.1
879.3
910 905 900 895 890 885 880 875
Binding Energy (eV)

Fig. 5

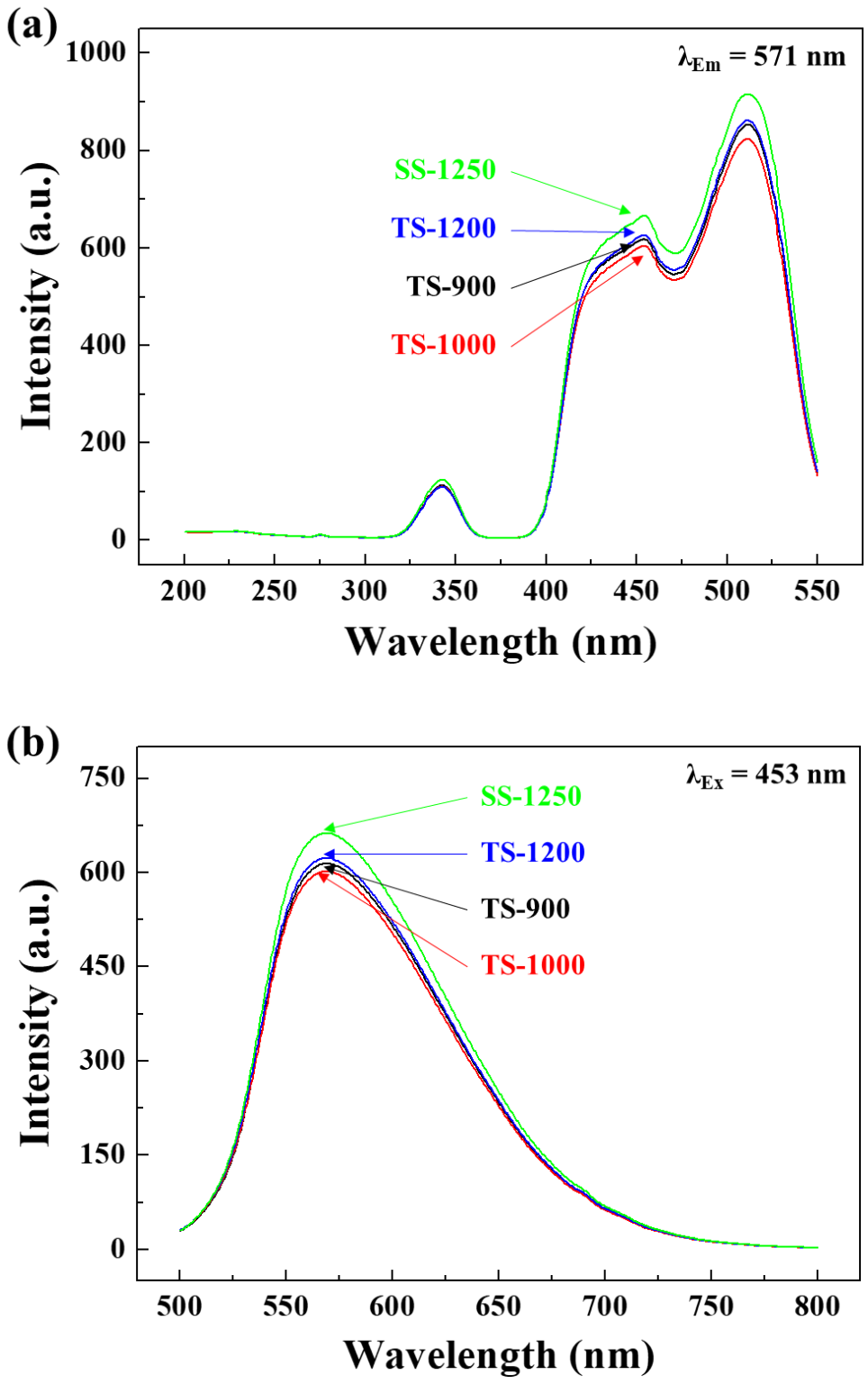
(a)
λEm = 571 nm
SS-1250
TS-1200
TS-900
TS-1000
Intensity (a.u.)
Wavelength (nm)
(b)
λEx = 453 nm
SS-1250
TS-1200
TS-900
TS-1000
Intensity (a.u.)
Wavelength (nm)

Fig. 6

Tables

Table 1. SPS conditions of the Ce^{3+}:$(Gd,Lu)_3Al_5O_{12}$ ceramics.

No.	Specimen name	SPS profile		Heating rate	Range (°C)	Holding stage
1	SS-1250	Single-step profile		50°C/min	600–1250	@ 1250°C for 20 min
2	TS-900	Two-step profile	1st step	50°C/min	600–900	@ 900°C for 30 min
			2nd step	5°C/min	900–1250	@ 1250°C for 20 min
3	TS-1000		1st step	50°C/min	600–1000	@ 1000°C for 30 min
			2nd step	5°C/min	1000–1250	@ 1250°C for 20 min
4	TS-1200		1st step	50°C/min	600–1200	@ 1200°C for 30 min
			2nd step	5°C/min	1200–1250	@ 1250°C for 20 min

Table 2. Microstructure parameters of the SPSed Ce^{3+}:$(Gd,Lu)_3Al_5O_{12}$ ceramics.

No.	Specimen name	Grain size	Pore size	Porosity
1	SS-1250	221 nm	81 nm	3.74%
2	TS-900	139 nm	43 nm	2.29%
3	TS-1000	163 nm	69 nm	1.63%
4	TS-1200	207 nm	72 nm	2.96%

Fabrication of transparent Ce^{3+}-doped $(Gd,Lu)_3Al_5O_{12}$ ceramics by two-step spark plasma sintering

Ji-Hwoan Lee[a], Byung-Nam Kim[a], Ji-Guang Li[a], and Byung-Koog Jang[b,*]

[a] Research Center for Functional Materials, National Institute for Materials Science, 1-2-1 Sengen, Tsukuba, Ibaraki 305-0047, Japan

[b] Interdisciplinary Graduate School of Engineering Science, Kyushu University, 6-1 Kasuga-koen, Kasuga, Fukuoka 816-8580, Japan

*Corresponding author:

E-mail address: jang.byungkoog@kyudai.jp (B.K. Jang)

Abstract

Transparent Ce^{3+}:$(Gd,Lu)_3Al_5O_{12}$ with microstructure control was fabricated by two-step spark plasma sintering. In the two-step profile, the heating rate was changed from 50 to 5°C/min at the first step temperatures. During the initial stage of shrinkage, the holding time of the first step sintering could induce densification by suppressing the microstructure coarsening. As compared to the single-step profile, the two-step profile showed a smaller grain size, which decreased with a decrease in the first step temperature. The porosity of the two-step profile was lower than that of the single-step profile, and the lowest porosity was obtained at the first step temperature of 1000°C, which was the starting point of shrinkage. The TS-1000 specimen showed the highest transmittance among all specimens because of the microstructure control offered by the two-step profile. Thus, by employing the two-step profile, the transmittance could be increased from 50.1% (SS-1250) to 56.5% (TS-1000).

Keywords: Two-step spark plasma sintering; Optical property; Photoluminescence characteristics; Microstructure; Gadolinium and lutetium aluminum garnet

1. Introduction

Lanthanide aluminum garnets ($Ln_3Al_5O_{12}$, LnAG), represented by $Gd_3Al_5O_{12}$ (GdAG) and $Lu_3Al_5O_{12}$ (LuAG), have high theoretical densities, and are attractive candidates for scintillator applications. LnAGs exhibit unique properties, such as wide bandgaps, high chemical and thermal stability, and a wide transparent range, which make them suitable for scintillator applications [1–4]. Scintillators should possess high theoretical density to stop X-rays. Yttrium aluminum garnet (YAG) shows relatively low X-ray stopping power due to its low density (4.53 g/cm^3). Among lanthanide elements with atomic weights higher than Y (89), Gd (157), and Lu (174) are considered suitable candidates for increasing the density of the garnet structure. However, Gd (0.21 ppm) and Lu (0.02 ppm) are less abundant in the earth's crust as compared to Y (1.39 ppm) [5]. As Gd is more abundant than Lu, it is considered to be a more suitable substitute for Y. Recently, transparent Gd-based LnAGs have been extensively investigated for scintillator applications. However, GdAGs thermally decompose into $GdAlO_3$ perovskite and Al_2O_3 above 1300°C ($Gd_3Al_5O_{12} \rightarrow 3GdAlO_3 + Al_2O_3$) [6]. In addition, GdAGs are doped with Ce^{3+} as an activator of yellow-emitting phosphors. The larger Ce^{3+} ions cause the destabilization of the garnet structure, thereby reducing its thermal decomposition temperature. In order to suppress their thermal decomposition, Ce-doped GdAGs are doped with Lu^{3+} ions, which are much smaller than Gd^{3+} ions [7]. These Lu^{3+} ions reduce the average Ln^{3+} size, and hence stabilize the garnet structure. In addition, Lu^{3+} doping retains the photoluminescence (PL) characteristics of Ce^{3+} and increases the theoretical density of Ce^{3+}:$(Gd,Lu)_3Al_5O_{12}$, thus enabling the development of advanced yellow-emitting phosphors [7].

Decreasing the sintering temperature can prevent the thermal decomposition of GdAG

above 1300°C and improve its mechanical properties while providing a dense microstructure. Among the various sintering techniques, spark plasma sintering (SPS) controlled by an electric field and mechanical pressure is considered to be an efficient sintering approach for GdAG [8,9]. In the SPS process, the electric field rapidly heats the mold and powder compact, facilitating rapid densification by several microscopic mechanisms, including increased atom diffusivity and softening of the particle surfaces, so that excessive grain growth is suppressed at low temperatures [8,10]. Therefore, high densities and fine microstructures, which are the advantages of SPS, improve the mechanical and optical properties of ceramics. Recently, the fabrication and characterization of LuAG ceramics, such as Nd:YAG [11], LuAG [12], and Ce^{3+}:$(Gd,Lu)_3Al_5O_{12}$ [13], using the SPS process have been reported [11–13]. Sufficient transparency can be obtained by conventional sintering, hot pressing (HP), and hot isostatic pressing (HIP) [14–16]. However, the fabrication of transparent LnAG using the SPS process has not been sufficiently studied. In our previous work [13], a Ce^{3+}:$(Gd,Lu)_3Al_5O_{12}$ powder was fully densified using the SPS process; however, a transparent compact was not obtained. Therefore, further research is required to improve the transparency of SPS-prepared ceramics while retaining the intrinsic merits of the SPS technique.

Various studies have reported the application of a two-step sintering profile to conventional sintering, HP, and HIP techniques to improve the optical properties and control the microstructure of ceramics [16–19]. Previous studies on the two-step sintering profile suggested that preliminary experiments on microstructure control should be conducted to improve the optical properties of ceramics [18,19]. Although the two-step sintering profile is applied in different ways, the main objective is to achieve primary densification without excessive coarsening at the higher first step temperature and full densification and removal

of residual pores during the second step sintering. As a result, full densification can be effectively achieved by dividing the sintering process into two steps with different objectives. In addition, some researchers have reported that a two-step profile can be applied to improve the optical properties of ceramics while retaining the intrinsic merits of the SPS process [20–24]. In the SPS process, the two-step profile is applied in a slightly different way, because the amounts of carbon contamination and residual pores inevitably increase with increased sintering time. Considerable research [22,23] has been carried out on the microstructure and optical properties of each step of the two-step profile. After primary densification without excessive microstructure coarsening when the first step temperature is lower than that of the second step, sufficient densification and excellent transparency could be achieved by removing the residual defects at the second step temperature. In our previous work [24], in transparent Y_2O_3 fabricated with a lower first step temperature, microstructural control and improved optical properties could be achieved. On the basis of the previously reported results regarding the two-step profile, it can be stated that by suppressing excessive microstructure coarsening and separating the primary densification and full densification processes, the microstructure of LnAG can be made fine and dense and its transmittance can be improved.

In the present work, the main objective is to control the microstructure and improve the optical properties by fabricating transparent Ce^{3+}:$(Gd,Lu)_3Al_5O_{12}$ ceramics by applying a two-step SPS profile. The two-step SPS profile is divided into first step (@ 900, 1000, and 1200°C) and second step (@ 1250°C) sintering, and the goals to be achieved in each step are as follows. At a relatively low temperature of first step sintering, primary densification can be achieved, which is effective in suppressing excessive microstructure coarsening. Next, in second step sintering, full densification and the removal of residual pores can be

accomplished. The microstructure and optical properties of the Ce^{3+}:$(Gd,Lu)_3Al_5O_{12}$ ceramics were evaluated by focusing on the improvement of in-line transmittance by varying the first step temperature.

2. Experimental Procedure

2.1. Preparation of Ce^{3+}:$(Gd,Lu)_3Al_5O_{12}$ powder

The rare-earth and aluminum sources used in this study were Ln_2O_3 (Ln = Gd and Lu, 99.99%, Huizhou RUIER Rare-Chem. Hi-Tech, China), $Ce(NO_3)_3 \cdot 6H_2O$ (99.99%, Huizhou RUIER Rare-Chem. Hi-Tech, China), and alum ($NH_4Al(SO_4)_2 \cdot 12H_2O$, > 99%, Zhenxin Chemical Reagent Factory, China). A $Ln(NO_3)_3$ stock solution was prepared by dissolving the oxide powders in an optimum amount of nitric acid. To precipitate the carbonate precursor, a mixed solution containing stoichiometric amounts of the nitrates and alum was added dropwise to the ammonium bicarbonate solution. The precipitated carbonate precursor was dried in an oven for 24 h. The $[(Gd_{0.6}Lu_{0.4})_{0.99}Ce_{0.01}]_3Al_5O_{12}$ powder was obtained by the thermal decomposition of the precursor *via* calcination at 1100°C for 4 h in air. To suppress the oxidation of Ce^{3+}, a second calcination process was performed at 1000°C for 4 h in Ar/H_2 (5 vol% of H_2) [7,25].

2.2. Consolidation of Ce^{3+}:$(Gd,Lu)_3Al_5O_{12}$ compacts using the SPS process

The Ce^{3+}:$(Gd,Lu)_3Al_5O_{12}$ powder was consolidated using SPS equipment (LABOX-315, Sinter Land, Japan) under a vacuum atmosphere of 10 Pa. The powder was directly sintered without any pretreatment, using a graphite mold with a diameter of 10 mm. Heating was performed using a pulse pattern of 5:5 (on:off) in the AC mode, and the temperature was measured by installing a pyrometer in the non-through hole of the mold. The entire SPS process was divided into single-step and two-step profiles. For the single-step profile, the powder compact was heated to a sintering temperature of 1250°C at a heating rate of 50°C/min, and held for 20 min. In the case of the two-step profile, to achieve primary

densification without excessive microstructure coarsening, first step sintering was performed at 900, 1000, and 1200°C with a heating rate of 50°C/min and the sintering temperature was held for 30 min. In the single-step profile, shrinkage started at approximately 1000°C. Thus, the first step temperature for the two-step profile was considered to be 1000°C. To achieve full densification and the removal of residual pores, further heating was conducted to reach the second step temperature of 1250°C at 5°C/min. This temperature was held for 20 min. In the entire SPS process, a mechanical pressure of 6.5 kN (80 MPa) was applied from the beginning and was maintained until cooling. In addition, cooling was sequentially performed at 1100°C for 10 min, 800°C for 5 min, and 25°C for 5 min. The SPS conditions and specimen names are listed in Table 1.

2.3. Characterization

The annealing process was conducted at 1250°C for 10 h in air to remove the carbon contamination and oxygen vacancies. Both of the surfaces of the Ce^{3+}:$(Gd,Lu)_3Al_5O_{12}$ compacts were mirror polished with 9, 3, and 1 μm diamond pastes. The transmittance of the compacts was measured using a double-beam spectrophotometer (SolidSpec-3700DUV, Shimazu, Japan) equipped with an integrating sphere. PL measurements were conducted using a spectrofluorometer (FP-6500, JASCO, Japan) equipped with a 60 mm diameter-integrating sphere (Model ISF-513, JASCO, Japan) and a 150 W Xe lamp as the excitation source. The X-ray photoelectron spectroscopy (XPS, AXIS-165, Shimadzu, Japan) profiles of the samples were recorded at room temperature with Al-K_α radiation for excitation. The binding energy was referenced to the C-1 s line of adventitious carbon. The mirror-polished surfaces were thermally etched at 1100°C for 2 h in air. The polished and fractured surfaces

of the specimens were examined using scanning electron microscopy (SEM, SU-8000, Hitachi, Japan). The porosity of the specimens was determined by measuring their porous areas from the SEM images. The grain and pore sizes of the specimens were calculated by measuring their pore sizes and average cross-sectional areas per grain. The grain size was apparent in the cross section; therefore, it was multiplied by 1.225 to determine the actual grain size [26].

3. Results and Discussion

3.1. Shrinkage behavior and microstructure

In our previous work, we successfully developed a stable $(Gd,Lu)_3Al_5O_{12}$ garnet structure, which could be well indexed to the cubic structure of GdAG [13]. Single-step and two-step SPS profiles were applied to fabricate transparent $(Gd,Lu)_3Al_5O_{12}$ ceramics with structural stabilization. The SPS curves (temperature, displacement, and pressure over time) of the single-step profile (SS-1250) are shown in Fig. 1 (a). As can be observed from the displacement curve, the ceramics showed thermal expansion when heated to approximately 1000°C. In addition, shrinkage began to occur at this temperature. No further shrinkage occurred during the holding period at 1250°C, and the shrinkage was sufficient. Based on the SPS curves of the single-step profile (SS-1250), a two-step profile (TS-1000) was designed, as shown in Fig. 1 (b). At a relatively low first step temperature of 1000°C, the powder compact was rapidly heated at 50°C/min to suppress excessive microstructure coarsening, and primary densification was performed for 30 min [20,22,24]. In addition, during the first step holding time, as the shrinkage began and did not occur rapidly, a small amount of residual pores could be expected. Owing to the achievement of primary densification, including a small amount of residual pores in the first step sintering, the shrinkage of the two-step profile was completed at 1200°C, which is approximately 50°C lower than that 1250°C of the single-step profile. However, the amount of shrinkage was almost the same. This improvement in the sintering behavior of the compacts by the two-step profile enabled microstructure control and improved the optical properties.

Fig. 2 shows the SEM images of the cross sections of the SPSed Ce^{3+}:$(Gd,Lu)_3Al_5O_{12}$ compacts after annealing. All specimens were densified at the final sintering temperature of

1250°C. However, the microstructures for the two SPS profiles differed in terms of grain size, pore size, and porosity. The microstructural parameters (grain size, pore size, and porosity) calculated from the SEM images are summarized in Table 2. Applying the two-step profile made it possible to significantly lower the porosity at the same sintering temperature. All two-step SPSed specimens showed lower porosity than that of the single-step SPSed specimen (SS-1250) (3.74%). In particular, the TS-1000 exhibited a porosity of 1.63%, indicating that a significant reduction in porosity was possible by applying the two-step SPS profile. The significant decrease in the porosity of the two-step SPSed specimens was due to improvement in their shrinkage behavior, i.e., fewer residual pores and a lower shrinkage-completion temperature, as shown in Fig. 2. In addition, as the first step temperature in the two-step profile was reduced, the grain size decreased gradually from 207 to 139 nm, and the pore size decreased from 72 to 43 nm. This microstructural change was due to the microstructure control of the two-step profile [18,19]. In this study, microstructure control using the two-step profile was expected to improve the optical properties as well.

3.2. Optical appearance and transmittance

The optical appearances of the Ce^{3+}:$(Gd,Lu)_3Al_5O_{12}$ compacts after annealing are shown in Fig. 3. The optical appearances and transparency of the annealed specimens placed on the grid can be easily compared. SS-1250 exhibited the lowest optical transparency among all specimens. Applying the modified two-step profile improved the optical appearance of the compacts. For two-step SPSed specimens, the optical appearance improved with a decrease in the heating rate at the second step. However, the most significant improvement was observed at the first step temperature of 1000°C. This indicates that a decrease in the heating

rate at the critical temperature for densification had a more significant effect than simply reducing the heating rate to improve the optical appearance. Therefore, at the first step temperature of 1000°C, porosity was lowest and the optical appearance also improved the most. The microstructure and optical appearance analysis results indicate that the TS-1000 specimen showed the highest transmittance among all specimens investigated in the present work.

Fig. 4 shows the in-line transmittance (ILT) curves of the sintered Ce^{3+}:$(Gd,Lu)_3Al_5O_{12}$ compacts after annealing. Significant light absorption was in the range of 420–500 nm. According to the reported results [27], well-fabricated $Lu_{2.7}Gd_{0.3}Al$-O_{12} ceramics exhibited excellent transmittance above 250 nm. In the present work, since light absorption by Ce^{3+} occurred at less than 500 nm, transmittance decreased rapidly. Owing to the light absorption due to the $4f \rightarrow 5d_2$ and $4f \rightarrow 5d_1$ transitions of Ce^{3+} at 340 nm and over a wavelength range of 420–500 nm, respectively, a strong light absorption band was detected [28]. The optical transmittance of the specimens showed the same trend as that of their optical appearance. At the same sintering temperature of 1250°C, all two-step SPSed specimens showed improved transmittance as compared to the single-step SPSed specimen. The TS-1000 specimen showed the most improved ILT of 56.5% at 1000 nm as compared to that (50.1%) of the SS-1250 specimen. In transparent ceramics, the area of the grain boundary also affects transmittance; however, porosity is the most critical factor [29]. In the case of the TS-1000 specimen, the first step temperature was 1000°C, at which shrinkage began, and porosity decreased significantly from 3.74% (SS-1250) to 1.63% (TS-1000). This decrease in porosity had a significant effect on the transmittance of the ceramic. In addition, as can be observed from Table 2, the porosity of the specimens showed a trend similar to that shown by the

optical transmittance. The TS-1000 specimen showed slightly reduced grain and pore sizes and significantly reduced porosity as compared to the SS-1250 specimen. The decrease in porosity, which had the most critical effect on transmittance, resulted in the most noticeable improvement in the transmittance of the TS-1000 specimen. $(Gd,Lu)_3Al_5O_{12}$:Ce ceramics with a composition similar to that of the ceramics prepared in this study were fabricated by conventional sintering at 1750°C for 4 h under a vacuum atmosphere after cold isostatic press at 240 MPa [14]. As a result, an ILT of approximately 72% was achieved at 1000 nm, showing excellent optical properties. Although there have been reports of preparing garnet materials with full densification and high transmittance by conventional sintering, it is difficult to achieve high transmittance with the SPS method. In a previous study, Nd:YAG ceramics were fabricated using the reactive-SPS method by applying a two-step heating profile [30]. The Nd:YAG powder was heated at 100°C/min to the first step temperature of 1000°C with an applied pressure of 70 MPa and at 15°C/min to the second step temperature of 1350°C, which was maintained for 5 min. However, an ILT of approximately 36% was obtained at 1000 nm, and excellent optical properties were not achieved. In this study, although the ILT was not close to the theoretical value, the transmittance could be improved through the application of the two-step profile and microstructure control.

3.3. Oxidation state and PL characteristic

XPS measurements were conducted to investigate the oxidation states of the Ce dopant, and the results of the powder, single-step profile (SS-1250), and two-step profile (TS-1000) are summarized in Fig. 5. The red lines represent the spectra of Ce^{3+} ions and the blue lines represent the spectra of Ce^{4+} ions. The fractions of the Ce^{3+} and Ce^{4+} ions were calculated

from the areas of their spectra. For comparing the as-synthesized powder with the compacts sintered in the single-step and two-step profiles, the fraction of Ce^{3+} in the as-synthesized powder was required. The fraction of Ce^{3+} in the powder was 61.42%, as shown in Fig. 5 (a). The Ce^{3+} fraction of the SS-1250 specimen was 61.73%, which is almost the same as that of the synthesized powder. However, because of slight oxidation, the TS-1000 specimen showed a Ce^{3+} fraction of 60.66%. As the SPS process provides an oxidizing atmosphere of graphite components, oxidation occurred in the two-step profile with a long sintering time, and the fraction of Ce^{3+} decreased slightly. The slightly decreased Ce^{3+} fraction of the two-step profile affected its PL characteristics along with the microstructure.

Fig. 6 (a) shows the PL excitation spectra of the Ce^{3+}:$(Gd,Lu)_3Al_5O_{12}$ compacts after annealing. PL excitation measurements were performed to investigate the wavelength-dependent excitation when 571 nm light was emitted. Excitation bands were detected at approximately 342, 453, and 506 nm, corresponding to the excitation of Ce^{3+} [31,32]. The excitation peak at approximately 342 nm correspond to the transition of Ce^{3+} from the ground state ($2F_{5/2}$) to the T_{2g} state. Excitation peaks at approximately 453 and 506 nm corresponded to the transition from the ground state to the E_{2g} state [31,32]. The SS-1250 specimen exhibited significantly higher PL excitation intensity than did the two-step profile specimens. Independent of the first step temperature, the PL excitation of the TS-1000 specimen intensity was the lowest. Their porosity strongly influenced the transmittance of the specimen, and the two-step profile showed better results than did the single-step profile. However, the PL excitation characteristics showed an opposite trend. First, the fraction of Ce^{3+} (Fig. 5) directly affected the PL excitation characteristics of the specimens. Because the PL excitation was caused only by Ce^{3+} [31,32], the fraction of Ce^{3+} present in the Ce^{3+}:$(Gd,Lu)_3Al_5O_{12}$ ceramics

was a very important factor. Next, the grain size of the SS-1250 specimen was the largest at 221 nm, which decreased gradually from 207 to 139 nm with a decrease in the first step temperature. Owing to its large grain size and small grain boundary area, the single-step profile affected the PL excitation characteristics of the compacts more than the two-step profile did [33,34]. Fig. 6 (b) shows the PL emission spectra of the Ce^{3+}:$(Gd,Lu)_3Al_5O_{12}$ compacts after annealing. The wavelength-dependent emission of the compacts under excitation by a wavelength of 453 nm was investigated. The PL emission characteristics of the compacts showed the same trend as that shown by the PL excitation characteristics. The full widths at half maximum values were almost the same for all specimens. This indicates that the crystallinity and light clarity of all specimens were almost the same and that the two-step profile did not affect the PL emission characteristics.

4. Conclusions

In this study, a two-step SPS profile was employed to improve the optical properties of Ce^{3+}:$(Gd,Lu)_3Al_5O_{12}$ ceramics as attractive yellow-emitting phosphors. The shrinkage curve of the two-step profile showed a significant reduction in porosity from 3.74% to 1.63% at the first step temperature of 1000°C, at which shrinkage began. As the first step temperature decreased, the microstructure control of the two-step profile refined the microstructure of the compacts by reducing the grain and pore sizes. As a result of the significant reduction in porosity in the two-step profile, transmittance improved from 50.1% to 56.5% at 1000 nm. On the other hand, oxidation occurred owing to the two-step profile's long sintering time, and the fraction of Ce^{3+} decreased slightly. Therefore, the two-step profile did not affect the ceramics' PL excitation and emission characteristics.

Acknowledgments

I would like to thank Dr. Craig A.J. Fisher of Japan Fine Ceramics Center (JFCC) for his constructive discussion on arranging and interpreting the transmittance and XPS results.

References

[1] J.G. Li, Y. Sakka, Recent progress in advanced optical materials based on gadolinium aluminate garnet ($Gd_3Al_5O_{12}$), Sci. Technol. Adv. Mater. 16 (2015) 014902.

[2] M. Wang, B. Lu, Manufacture and Faraday magneto-optical effect of highly transparent novel holmium aluminum garnet ceramics, Scripta Mater. 195 (2021) 133729.

[3] I. Milisavljevic, G. Zhang, Y. Wu, Solid-state single-crystal growth of YAG and Nd: YAG by spark plasma sintering, J. Mater. Sci. Technol. 106 (2022) 118–127.

[4] C. Kim, W. Lee, A. Melis, A. Elmughrabi, K. Lee, C. Park, J.Y. Yeom, A Review of Inorganic Scintillation Crystals for Extreme Environments, Crystals 11 (2021) 669.

[5] V. Balaram, Rare earth elements: A review of applications, occurrence, exploration, analysis, recycling, and environmental impact, Geosci. Front. 10 (2019) 1285–1303.

[6] T. Shishido, K. Okamura, S. Yajima, $Gd_3Al_5O_{12}$ Phase Obtained by Crystallization of Amorphous $Gd_2O_3 \cdot 5/3Al_2O_3$, J. Am. Ceram. Soc. 61 (1978) 373–375.

[7] J. Li, J.G. Li, S. Liu, X. Li, X. Sun, Y. Sakka, The development of Ce^{3+}-activated $(Gd,Lu)_3Al_5O_{12}$ garnet solid solutions as efficient yellow-emitting phosphors, Sci. Technol. Adv. Mater. 14 (2013) 054201.

[8] B.N. Kim, K. Morita, T.S. Suzuki, J.G. Li, H. Matsubara, Simulation of densification behavior of nano-powder in final sintering stage: Effect of pore-size distribution, J. Eur. Ceram. Soc. 41 (2021) 625–634.

[9] M. Tokita, Progress of Spark Plasma Sintering (SPS) Method, Systems, Ceramics Applications and Industrialization, Ceramics 4 (2021) 160–198.

[10] A. Wagner, Y. Meshorer, B. Ratzker, D. Sinefeld, S. Kalabukhov, S. Goldring, E.

Galun, N. Frage, Pressure‐assisted sintering and characterization of Nd:YAG ceramic lasers, Sci. Rep. 11 (2021) 1512.

[11] A. Wagner, B. Ratzker, S. Kalabukhov, S. Kolusheva, M. Sokol, N. Frage, Highly-doped Nd:YAG ceramics fabricated by conventional and high pressure SPS, Ceram. Int. 45 (2019) 12279–12284.

[12] S.F. Wang, J. Zhang, D.W. Luo, F. Gu, D.Y. Tang, Z.L. Dong, G.E.B. Tan, W.X. Que, T.S. Zhang, S. Li, L.B. Kong, Transparent ceramics: Processing, materials and applications, Prog. Solid. State. Chem. 41 (2013) 20–54.

[13] J.H. Lee, J.G. Li, B.N. Kim, Q. Meng, X. Sun, B.K. Jang, Effect of annealing on microstructure and luminescence characteristics in spark plasma sintered Ce^{3+}-activated $(Gd,Lu)_3Al_5O_{12}$ garnet ceramics, J. Eur. Ceram. Soc. 41 (2021) 1586–1592.

[14] Z. Sun, Z. Chen, M. Wang, B. Lu, Production and optical properties of Ce^{3+}-activated and Lu^{3+}-stabilized transparent gadolinium aluminate garnet ceramics, J. Am. Ceram. Soc. 103 (2020) 809–818.

[15] X. Chen, X. Liu, Y. Feng, X. Li, H. Chen, T. Xie, H. Kou, R. Kucerkova, Microstructure evolution in two-step-sintering process toward transparent Ce:$(Y,Gd)_3(Ga,Al)_5O_{12}$ scintillation ceramics. J. Alloys Compd. 846 (2020) 156377.

[16] J. Li, Q. Chen, G. Feng, W. Wu, D. Xiao, J. Zhu, Optical properties of the polycrystalline transparent Nd:YAG ceramics prepared by two-step sintering, Ceram. Int. 38S (2012) S649–S652.

[17] Z. Seeley, N. Cherepy, S. Payne, Two-step sintering of $Gd_{0.3}Lu_{1.6}Eu_{0.1}O_3$ transparent ceramic scintillator, Opt. Mater. Express. 3 (2013) 908–912.

[18] W.K. Jung, H.J. Ma, D.G. Kim, D.K. Kim, Two-step sintering behavior of titanium-

doped Y_2O_3 ceramics with monodispersed sub-micrometer powder, Ceram. Int. 45 (2019) 510–515.

[19] H.J. Ma, W.K. Jung, C. Baek, D.K. Kim, Influence of microstructure control on optical and mechanical properties of infrared transparent Y_2O_3-MgO nanocomposite, J. Eur. Ceram. Soc. 37 (2017) 4902–4911.

[20] H. Furuse, S. Nakasawa, H. Yoshida, K. Morita, T.S. Suzuki, B.N. Kim, Y. Sakka, K. Hiraga, Transparent ultrafine Yb^{3+}:Y_2O_3 laser ceramics fabricated by spark plasma sintering, J. Am. Ceram. Soc. 101 (2018) 694–702.

[21] K. Morita, B.N. Kim, H. Yoshida, H. Zhang, K. Hiraga, Y. Sakka, Effect of loading schedule on densification of $MgAl_2O_4$ spinel during spark plasma sintering (SPS) processing, J. Eur. Ceram. Soc. 32 (2012) 2303–2309.

[22] M. Nanko, K.Q. Dan, Two-step pulsed electric current sintering of transparent Al_2O_3 ceramics, Adv. Appl. Ceram. 113 (2014) 80–84.

[23] H.H. Nguyen, M. Nanko, Densification and grain growth of large-sized polycrystalline Al_2O_3 during a two-step pulsed electric current sintering process, Mater. Trans. 59 (2018) 1610–1615.

[24] J.H. Lee, B.N. Kim, B.K. Jang, Fabrication of transparent Y_2O_3 ceramics by two-step spark plasma sintering, J. Am. Ceram. Soc. 104 (2021) 5501–5508.

[25] J. Li, J.G. Li, X. Li, X. Sun, Photoluminescence properties of phosphors based on Lu^{3+}-stabilized $Gd_3Al_5O_{12}$:Tb^{3+}/Ce^{3+} garnet solid solutions, Opt. Mater. 62 (2016) 328–334.

[26] S. Grasso, C. Hu, G. Maizza, B.N. Kim, Y. Sakka, Effects of pressure application method on transparency of spark plasma sintered alumina, J. Am. Ceram. Soc. 94 (2011) 1405–1409.

[27] P. Ma, T. Xie, L. Wu, H. Chen, H. Kou, Y. Shi, Y. Pan, J. Li, Fabrication of Nd:$Lu_{2.7}Gd_{0.3}Al_5O_{12}$ transparent ceramics by solid-state reactive sintering, Opt. Mater. 66 (2017) 422–427.

[28] S. Feng, H. Qin, G. Wu, H. Jiang, J. Zhao, Y. Liu, Z. Luo, J. Qioa, J. Jiang, Spectrum regulation of YAG:Ce transparent ceramics with Pr, Cr doping for white light emitting diodes application, J. Eur. Ceram. Soc. 37 (2017) 3403–3409.

[29] T. Benitez, S.Y. Gomez, A. Oliveira, N. Travitzky, D. Hotza, Transparent ceramic and glass-ceramic materials for armor applications, Ceram. Int. 43 (2017) 13031–13046.

[30] D.Y. Kosyanov, A.A. Vornovskikh, A.M. Zakharenko, E.A. Gridasova, R.P. Yavetskiy, M.V. Dobrotvorskaya, A.V. Tolmachev, O.O. Shichalin, E.K. Papynov, A.Y. Ustinov, V.G. Kuryavyi, A.A. Leonov, S.A. Tikhonov, Influence of sintering parameters on transparency of reactive SPSed Nd^{3+}:YAG ceramics, Opt. Mater. 112 (2021) 110760.

[31] X. Su, K. Zhang, Q. Liu, H. Zhong, Y. Shi, Y. Pan, Combinatorial Optimization of $(Lu_{1-x}Gd_x)_3Al_5O_{12}$:$Ce_{3y}$ Yellow Phosphors as Precursors for Ceramic Scintillators, ACS Comb. Sci. 13 (2011) 79–83.

[32] A. Birkel, K.A. Denault, N.C. George, C.E. Doll, B. Hery, A.A. Mikhailovsky, C.S. Birkel, B.C. Hong, R. Seshadri, Rapid Microwave Preparation of Highly Efficient Ce^{3+}-Substituted Garnet Phosphors for Solid State White Lighting, Chem. Mater. 24 (2012) 1198–1204.

[33] B. Wen, D.F. Zhang, N. Zhang, J.K. Feng, B. Jiang, F.S. Pan, Y. Zhang, L. Yang, Effect of grain size on the luminescent properties of Ce^{3+} doped $Y_3Al_5O_{12}$ ceramic phosphor plates, Ceram. Int. 46 (2020) 10452–10456.

[34] Y. Kim, S. Jang, Effect of particle size on photoluminescence emission intensity of

ZnO, Acta Mater. 59 (2011) 3024–3031.

Figure captions

Figure 1. SPS curves of the SPSed Ce^{3+}:$(Gd,Lu)_3Al_5O_{12}$ ceramics (a) single-step SPS (SS-1250) and (b) two-step SPS (TS-1000).

Figure 2. SEM images of the cross sections of the SPSed Ce^{3+}:$(Gd,Lu)_3Al_5O_{12}$ ceramics.

Figure 3. Optical appearances of the SPSed Ce^{3+}:$(Gd,Lu)_3Al_5O_{12}$ ceramics under the conditions listed in Table 1.

Figure 4. (a) Transmittance curves of the SPSed Ce^{3+}:$(Gd,Lu)_3Al_5O_{12}$ ceramics after annealing; (b) the curve magnified over the wavelength of 750–1050 nm.

Figure 5. XPS profiles of the (a) Ce^{3+}:$(Gd,Lu)_3Al_5O_{12}$ powder, (b) single-step SPSed compact (SS-1250), and (c) two-step SPSed compact (TS-1000).

Figure 6. (a) PL excitation and (b) PL emission spectra of Ce^{3+}:$(Gd,Lu)_3Al_5O_{12}$ ceramics with different SPS conditions after annealing.

Figures

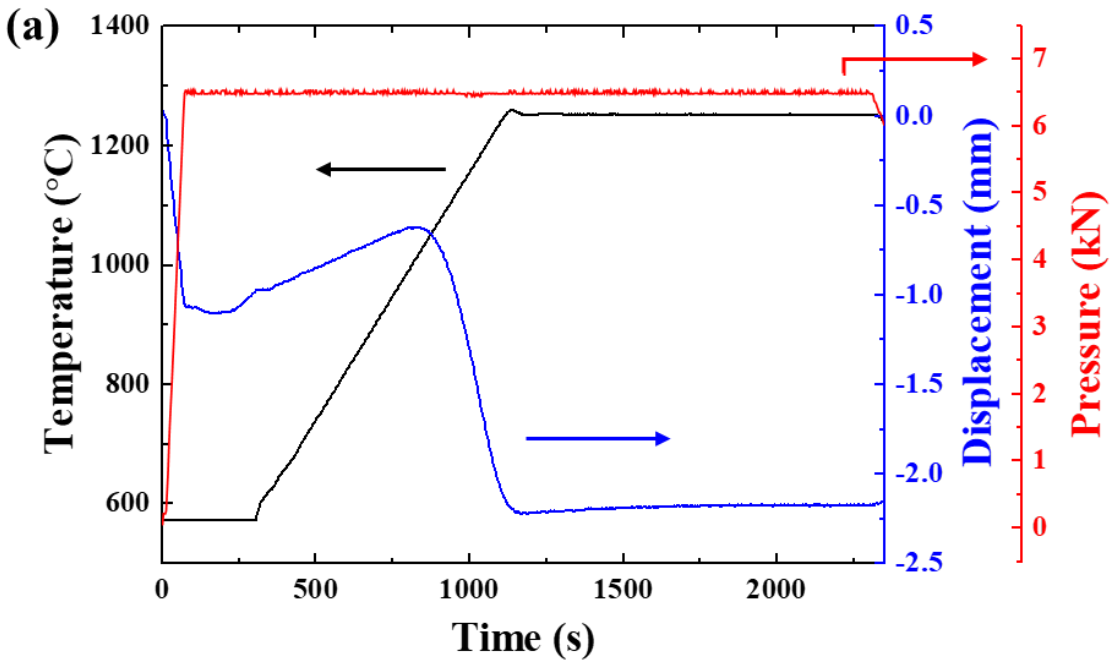

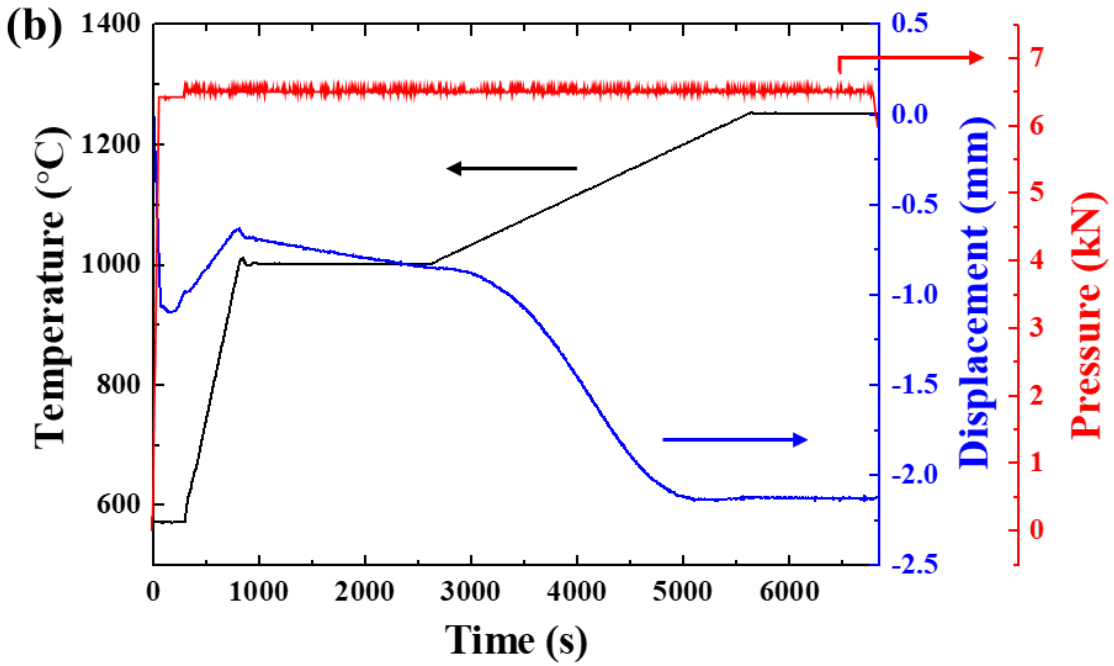

Fig. 1

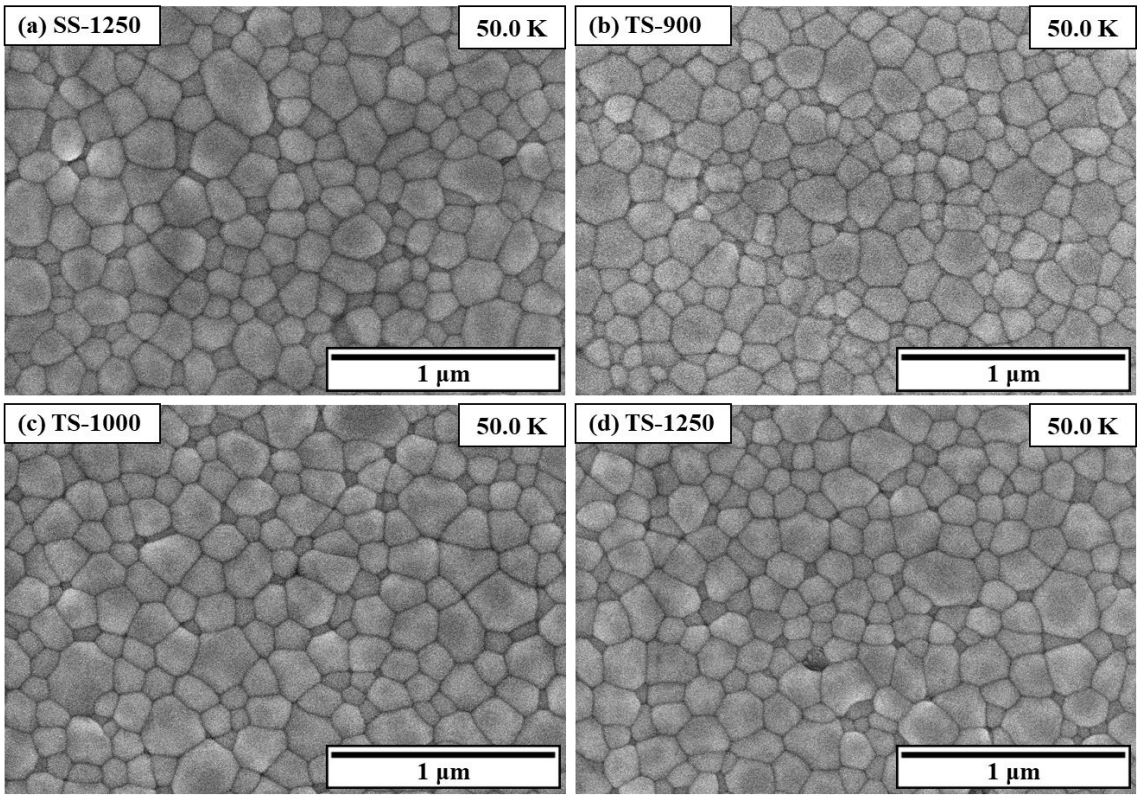
(a) SS-1250
50.0 K
1 µm
(b) TS-900
50.0 K
1 µm
(c) TS-1000
50.0 K
1 µm
(d) TS-1250
50.0 K
1 µm

Fig. 2

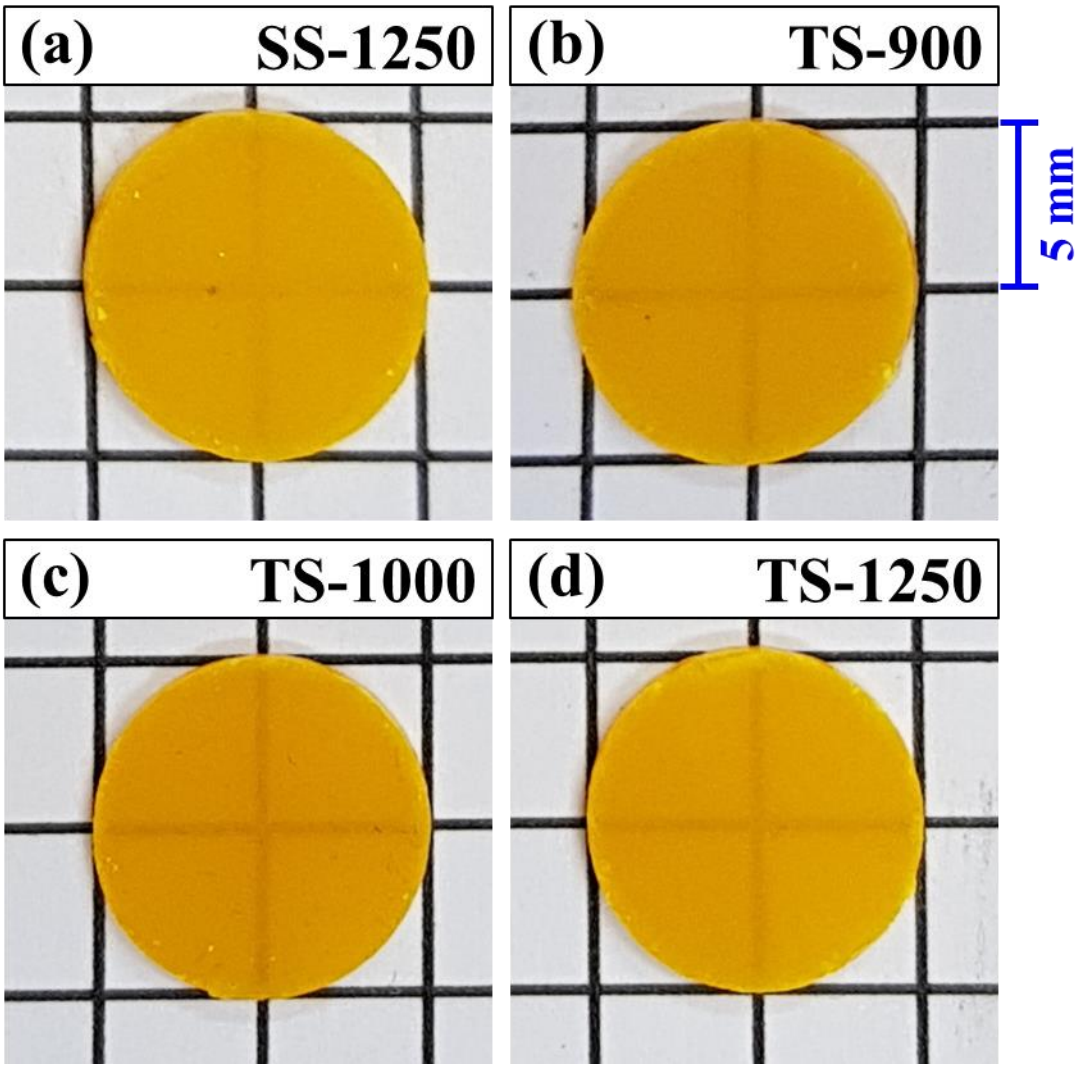

Fig. 3

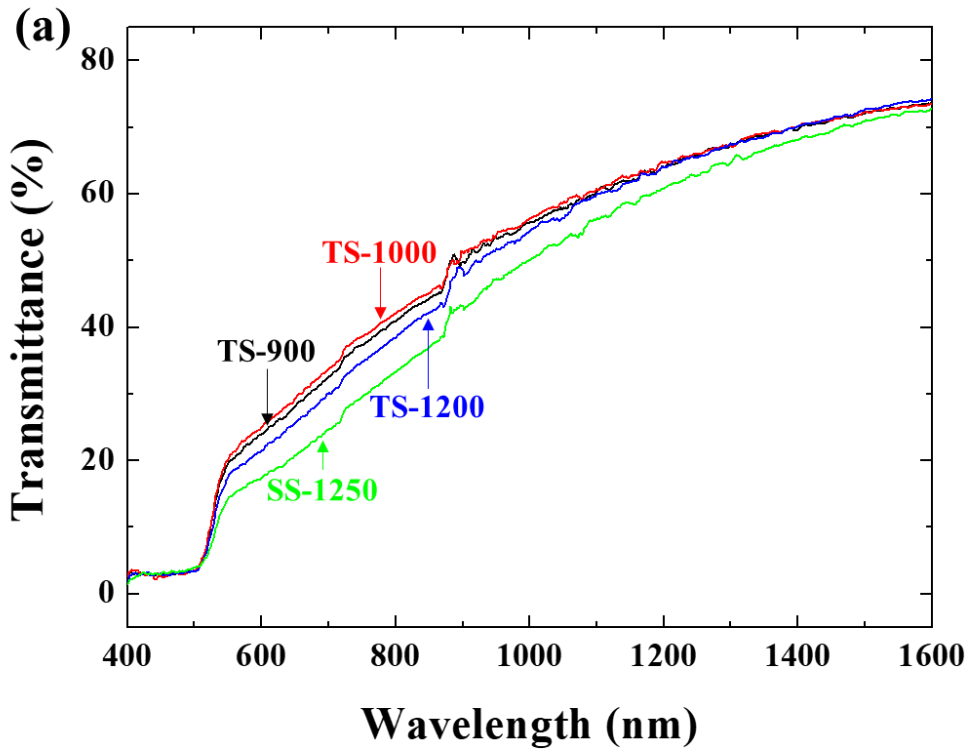
(a)
Transmittance (%)
Wavelength (nm)
TS-1000
TS-900
TS-1200
SS-1250
0
20
40
60
80
400
600
800
1000
1200
1400
1600

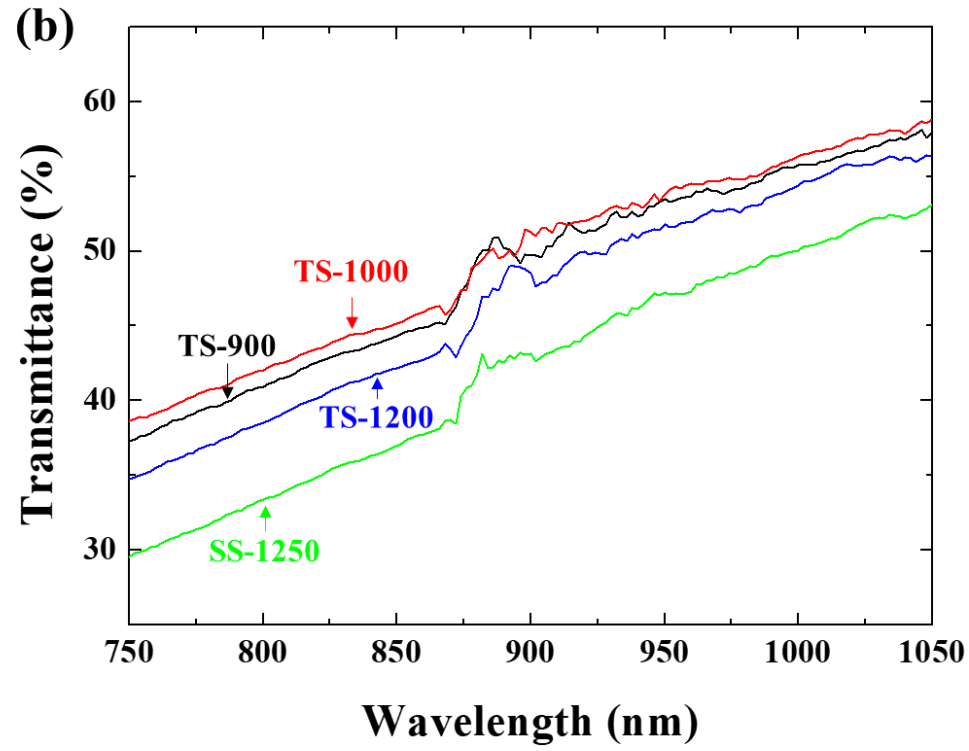
(b)
Transmittance (%)
Wavelength (nm)
TS-1000
TS-900
TS-1200
SS-1250
30
40
50
60
750
800
850
900
950
1000
1050

Fig. 4

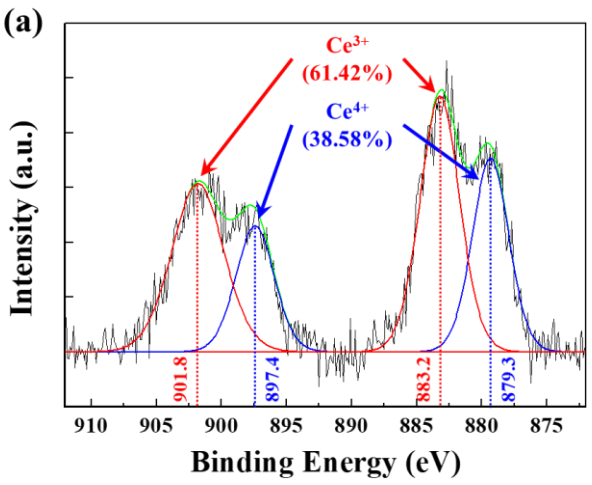
(a)
Ce3+
(61.42%)
Ce4+
(38.58%)
Intensity (a.u.)
901.8
897.4
883.2
879.3
910 905 900 895 890 885 880 875
Binding Energy (eV)

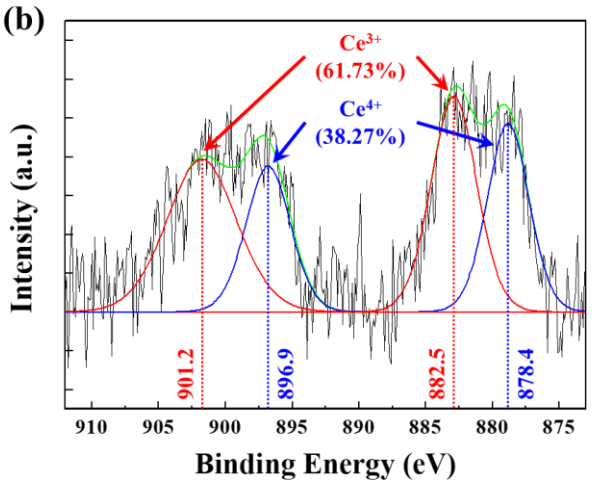
(b)
Ce3+
(61.73%)
Ce4+
(38.27%)
Intensity (a.u.)
901.2
896.9
882.5
878.4
910 905 900 895 890 885 880 875
Binding Energy (eV)

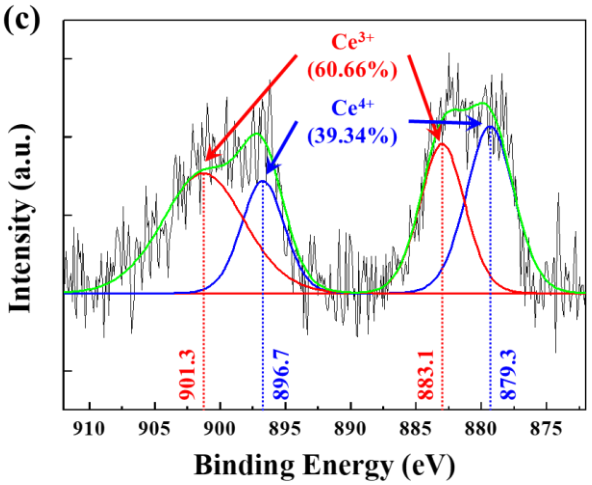
(c)
Ce3+
(60.66%)
Ce4+
(39.34%)
Intensity (a.u.)
901.3
896.7
883.1
879.3
910 905 900 895 890 885 880 875
Binding Energy (eV)

Fig. 5

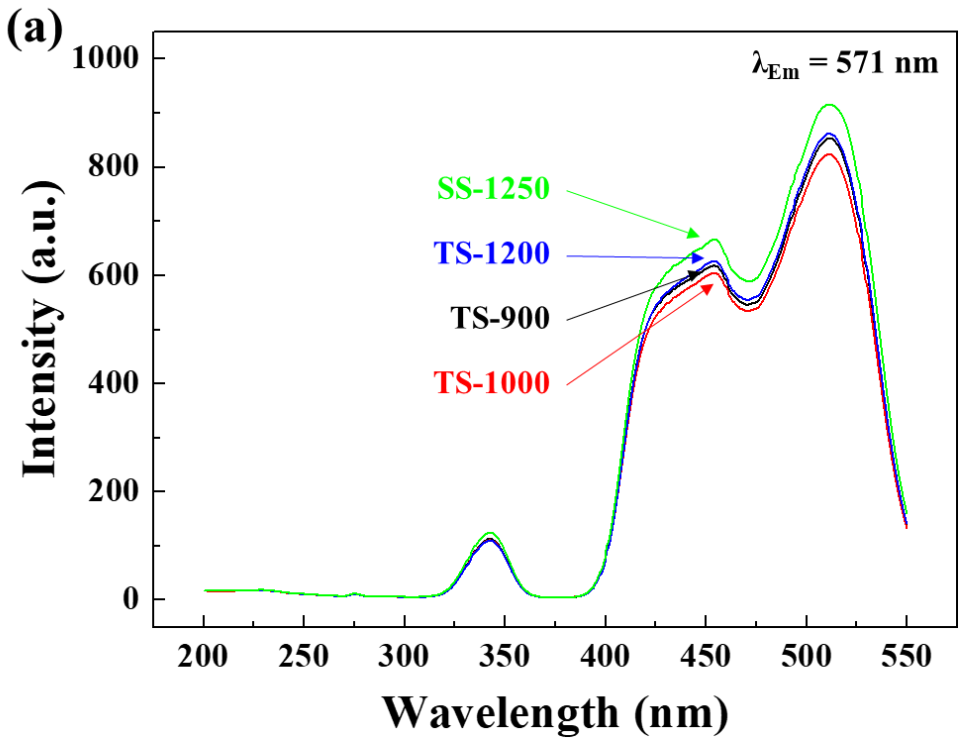
(a)
λEm = 571 nm
SS-1250
TS-1200
TS-900
TS-1000
Intensity (a.u.)
Wavelength (nm)
0
200
400
600
800
1000
200
250
300
350
400
450
500
550

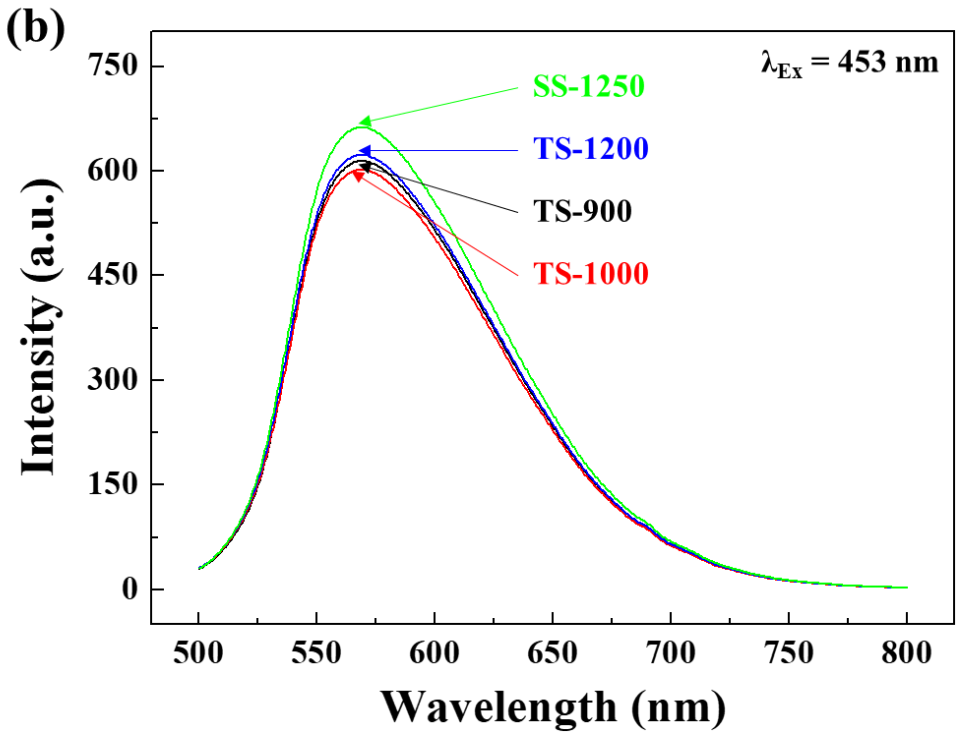
(b)
λEx = 453 nm
SS-1250
TS-1200
TS-900
TS-1000
Intensity (a.u.)
Wavelength (nm)
0
150
300
450
600
750
500
550
600
650
700
750
800

Fig. 6

Tables

Table 1. SPS conditions of Ce^{3+}:$(Gd,Lu)_3Al_5O_{12}$ ceramics.

No.	Specimen name	SPS profile		Heating rate	Range (°C)	Holding stage
1	SS-1250	Single-step profile		50°C/min	600–1250	@ 1250°C for 20 min
2	TS-900	Two-step profile	1st step	50°C/min	600–900	@ 900°C for 30 min
			2nd step	5°C/min	900–1250	@ 1250°C for 20 min
3	TS-1000		1st step	50°C/min	600–1000	@ 1000°C for 30 min
			2nd step	5°C/min	1000–1250	@ 1250°C for 20 min
4	TS-1200		1st step	50°C/min	600–1200	@ 1200°C for 30 min
			2nd step	5°C/min	1200–1250	@ 1250°C for 20 min

Table 2. Microstructure parameters of SPSed Ce^{3+}:$(Gd,Lu)_3Al_5O_{12}$ ceramics.

No.	Specimen name	Grain size	Pore size	Porosity
1	SS-1250	221 nm	81 nm	3.74%
2	TS-900	139 nm	43 nm	2.29%
3	TS-1000	163 nm	69 nm	1.63%
4	TS-1200	207 nm	72 nm	2.96%

Fabrication of transparent Ce^{3+}-doped $(Gd,Lu)_3Al_5O_{12}$ ceramics by two-step spark plasma sintering

Ji-Hwoan Lee[a], Byung-Nam Kim[a], Ji-Guang Li[a], and Byung-Koog Jang[b,*]

[a] Research Center for Functional Materials, National Institute for Materials Science, 1-2-1 Sengen, Tsukuba, Ibaraki 305-0047, Japan

[b] Interdisciplinary Graduate School of Engineering Science, Kyushu University, 6-1 Kasuga-koen, Kasuga, Fukuoka 816-8580, Japan

*Corresponding author:

E-mail address: jang.byungkoog@kyudai.jp (B.K. Jang)

Abstract

Transparent Ce^{3+}:$(Gd,Lu)_3Al_5O_{12}$ with microstructure control was fabricated by two-step spark plasma sintering. In the two-step profile, the heating rate was changed from 50 to 5°C/min at the first step temperatures. During the initial stage of shrinkage, the holding time of the first step sintering could induce densification by suppressing the microstructure coarsening. As compared to the single-step profile, the two-step profile showed a smaller grain size, which decreased with a decrease in the first step temperature. The porosity of the two-step profile was lower than that of the single-step profile, and the lowest porosity was obtained at the first step temperature of 1000°C, which was the starting point of shrinkage. The TS-1000 specimen showed the highest transmittance among all specimens because of the microstructure control offered by the two-step profile. Thus, by employing the two-step profile, the transmittance could be increased from 50.1% (SS-1250) to 56.5% (TS-1000).

Keywords: Two-step spark plasma sintering; Optical property; Photoluminescence characteristics; Microstructure; Gadolinium and lutetium aluminum garnet

1. Introduction

Lanthanide aluminum garnets ($Ln_3Al_5O_{12}$, LnAG), represented by $Gd_3Al_5O_{12}$ (GdAG) and $Lu_3Al_5O_{12}$ (LuAG), have high theoretical densities, and are attractive candidates for scintillator applications. LnAGs exhibit unique properties, such as wide bandgaps, high chemical and thermal stability, and a wide transparent range, which make them suitable for scintillator applications [1–4]. Scintillators should possess high theoretical density to stop X-rays. Yttrium aluminum garnet (YAG) shows relatively low X-ray stopping power due to its low density (4.53 g/cm^3). Among lanthanide elements with atomic weights higher than Y (89), Gd (157), and Lu (174) are considered suitable candidates for increasing the density of the garnet structure. However, Gd (0.21 ppm) and Lu (0.02 ppm) are less abundant in the earth's crust as compared to Y (1.39 ppm) [5]. As Gd is more abundant than Lu, it is considered to be a more suitable substitute for Y. Recently, transparent Gd-based LnAGs have been extensively investigated for scintillator applications. However, GdAGs thermally decompose into $GdAlO_3$ perovskite and Al_2O_3 above 1300°C ($Gd_3Al_5O_{12} \rightarrow 3GdAlO_3 + Al_2O_3$) [6]. In addition, GdAGs are doped with Ce^{3+} as an activator of yellow-emitting phosphors. The larger Ce^{3+} ions cause the destabilization of the garnet structure, thereby reducing its thermal decomposition temperature. In order to suppress their thermal decomposition, Ce-doped GdAGs are doped with Lu^{3+} ions, which are much smaller than Gd^{3+} ions [7]. These Lu^{3+} ions reduce the average Ln^{3+} size, and hence stabilize the garnet structure. In addition, Lu^{3+} doping retains the photoluminescence (PL) characteristics of Ce^{3+} and increases the theoretical density of Ce^{3+}:$(Gd,Lu)_3Al_5O_{12}$, thus enabling the development of advanced yellow-emitting phosphors [7].

Decreasing the sintering temperature can prevent the thermal decomposition of GdAG

above 1300°C and improve its mechanical properties while providing a dense microstructure. Among the various sintering techniques, spark plasma sintering (SPS) controlled by an electric field and mechanical pressure is considered to be an efficient sintering approach for GdAG [8,9]. In the SPS process, the electric field rapidly heats the mold and powder compact, facilitating rapid densification by several microscopic mechanisms, including increased atom diffusivity and softening of the particle surfaces, so that excessive grain growth is suppressed at low temperatures [8,10]. Therefore, high densities and fine microstructures, which are the advantages of SPS, improve the mechanical and optical properties of ceramics. Recently, the fabrication and characterization of LuAG ceramics, such as Nd:YAG [11], LuAG [12], and Ce^{3+}:$(Gd,Lu)_3Al_5O_{12}$ [13], using the SPS process have been reported [11–13]. Sufficient transparency can be obtained by conventional sintering, hot pressing (HP), and hot isostatic pressing (HIP) [14–16]. However, the fabrication of transparent LnAG using the SPS process has not been sufficiently studied. In our previous work [13], a Ce^{3+}:$(Gd,Lu)_3Al_5O_{12}$ powder was fully densified using the SPS process; however, a transparent compact was not obtained. Therefore, further research is required to improve the transparency of SPS-prepared ceramics while retaining the intrinsic merits of the SPS technique.

Various studies have reported the application of a two-step sintering profile to conventional sintering, HP, and HIP techniques to improve the optical properties and control the microstructure of ceramics [16–19]. Previous studies on the two-step sintering profile suggested that preliminary experiments on microstructure control should be conducted to improve the optical properties of ceramics [18,19]. Although the two-step sintering profile is applied in different ways, the main objective is to achieve primary densification without excessive coarsening at the higher first step temperature and full densification and removal

of residual pores during the second step sintering. As a result, full densification can be effectively achieved by dividing the sintering process into two steps with different objectives. In addition, some researchers have reported that a two-step profile can be applied to improve the optical properties of ceramics while retaining the intrinsic merits of the SPS process [20–24]. In the SPS process, the two-step profile is applied in a slightly different way, because the amounts of carbon contamination and residual pores inevitably increase with increased sintering time. Considerable research [22,23] has been carried out on the microstructure and optical properties of each step of the two-step profile. After primary densification without excessive microstructure coarsening when the first step temperature is lower than that of the second step, sufficient densification and excellent transparency could be achieved by removing the residual defects at the second step temperature. In our previous work [24], in transparent Y_2O_3 fabricated with a lower first step temperature, microstructural control and improved optical properties could be achieved. On the basis of the previously reported results regarding the two-step profile, it can be stated that by suppressing excessive microstructure coarsening and separating the primary densification and full densification processes, the microstructure of LnAG can be made fine and dense and its transmittance can be improved.

In the present work, the main objective is to control the microstructure and improve the optical properties by fabricating transparent Ce^{3+}:$(Gd,Lu)_3Al_5O_{12}$ ceramics by applying a two-step SPS profile. The two-step SPS profile is divided into first step (@ 900, 1000, and 1200°C) and second step (@ 1250°C) sintering, and the goals to be achieved in each step are as follows. At a relatively low temperature of first step sintering, primary densification can be achieved, which is effective in suppressing excessive microstructure coarsening. Next, in second step sintering, full densification and the removal of residual pores can be

accomplished. The microstructure and optical properties of the Ce^{3+}:$(Gd,Lu)_3Al_5O_{12}$ ceramics were evaluated by focusing on the improvement of in-line transmittance by varying the first step temperature.

2. Experimental Procedure

2.1. Preparation of Ce^{3+}:$(Gd,Lu)_3Al_5O_{12}$ powder

The rare-earth and aluminum sources used in this study were Ln_2O_3 (Ln = Gd and Lu, 99.99%, Huizhou RUIER Rare-Chem. Hi-Tech, China), $Ce(NO_3)_3 \cdot 6H_2O$ (99.99%, Huizhou RUIER Rare-Chem. Hi-Tech, China), and alum ($NH_4Al(SO_4)_2 \cdot 12H_2O$, > 99%, Zhenxin Chemical Reagent Factory, China). A $Ln(NO_3)_3$ stock solution was prepared by dissolving the oxide powders in an optimum amount of nitric acid. To precipitate the carbonate precursor, a mixed solution containing stoichiometric amounts of the nitrates and alum was added dropwise to the ammonium bicarbonate solution. The precipitated carbonate precursor was dried in an oven for 24 h. The $[(Gd_{0.6}Lu_{0.4})_{0.99}Ce_{0.01}]_3Al_5O_{12}$ powder was obtained by the thermal decomposition of the precursor *via* calcination at 1100°C for 4 h in air. To suppress the oxidation of Ce^{3+}, a second calcination process was performed at 1000°C for 4 h in Ar/H_2 (5 vol% of H_2) [7,25].

2.2. Consolidation of Ce^{3+}:$(Gd,Lu)_3Al_5O_{12}$ compacts using the SPS process

The Ce^{3+}:$(Gd,Lu)_3Al_5O_{12}$ powder was consolidated using SPS equipment (LABOX-315, Sinter Land, Japan) under a vacuum atmosphere of 10 Pa. The powder was directly sintered without any pretreatment, using a graphite mold with a diameter of 10 mm. Heating was performed using a pulse pattern of 5:5 (on:off) in the AC mode, and the temperature was measured by installing a pyrometer in the non-through hole of the mold. The entire SPS process was divided into single-step and two-step profiles. For the single-step profile, the powder compact was heated to a sintering temperature of 1250°C at a heating rate of 50°C/min, and held for 20 min. In the case of the two-step profile, to achieve primary

densification without excessive microstructure coarsening, first step sintering was performed at 900, 1000, and 1200°C with a heating rate of 50°C/min and the sintering temperature was held for 30 min. In the single-step profile, shrinkage started at approximately 1000°C. Thus, the first step temperature for the two-step profile was considered to be 1000°C. To achieve full densification and the removal of residual pores, further heating was conducted to reach the second step temperature of 1250°C at 5°C/min. This temperature was held for 20 min. In the entire SPS process, a mechanical pressure of 6.5 kN (80 MPa) was applied from the beginning and was maintained until cooling. In addition, cooling was sequentially performed at 1100°C for 10 min, 800°C for 5 min, and 25°C for 5 min. The SPS conditions and specimen names are listed in Table 1.

2.3. Characterization

The annealing process was conducted at 1250°C for 10 h in air to remove the carbon contamination and oxygen vacancies. Both of the surfaces of the Ce^{3+}:$(Gd,Lu)_3Al_5O_{12}$ compacts were mirror polished with 9, 3, and 1 μm diamond pastes. The transmittance of the compacts was measured using a double-beam spectrophotometer (SolidSpec-3700DUV, Shimazu, Japan) equipped with an integrating sphere. PL measurements were conducted using a spectrofluorometer (FP-6500, JASCO, Japan) equipped with a 60 mm diameter-integrating sphere (Model ISF-513, JASCO, Japan) and a 150 W Xe lamp as the excitation source. The X-ray photoelectron spectroscopy (XPS, AXIS-165, Shimadzu, Japan) profiles of the samples were recorded at room temperature with Al-K_α radiation for excitation. The binding energy was referenced to the C-1 s line of adventitious carbon. The mirror-polished surfaces were thermally etched at 1100°C for 2 h in air. The polished and fractured surfaces

of the specimens were examined using scanning electron microscopy (SEM, SU-8000, Hitachi, Japan). The porosity of the specimens was determined by measuring their porous areas from the SEM images. The grain and pore sizes of the specimens were calculated by measuring their pore sizes and average cross-sectional areas per grain. The grain size was apparent in the cross section; therefore, it was multiplied by 1.225 to determine the actual grain size [26].

3. Results and Discussion

3.1. Shrinkage behavior and microstructure

In our previous work, we successfully developed a stable $(Gd,Lu)_3Al_5O_{12}$ garnet structure, which could be well indexed to the cubic structure of GdAG [13]. Single-step and two-step SPS profiles were applied to fabricate transparent $(Gd,Lu)_3Al_5O_{12}$ ceramics with structural stabilization. The SPS curves (temperature, displacement, and pressure over time) of the single-step profile (SS-1250) are shown in Fig. 1 (a). As can be observed from the displacement curve, the ceramics showed thermal expansion when heated to approximately 1000°C. In addition, shrinkage began to occur at this temperature. No further shrinkage occurred during the holding period at 1250°C, and the shrinkage was sufficient. Based on the SPS curves of the single-step profile (SS-1250), a two-step profile (TS-1000) was designed, as shown in Fig. 1 (b). At a relatively low first step temperature of 1000°C, the powder compact was rapidly heated at 50°C/min to suppress excessive microstructure coarsening, and primary densification was performed for 30 min [20,22,24]. In addition, during the first step holding time, as the shrinkage began and did not occur rapidly, a small amount of residual pores could be expected. Owing to the achievement of primary densification, including a small amount of residual pores in the first step sintering, the shrinkage of the two-step profile was completed at 1200°C, which is approximately 50°C lower than that 1250°C of the single-step profile. However, the amount of shrinkage was almost the same. This improvement in the sintering behavior of the compacts by the two-step profile enabled microstructure control and improved the optical properties.

Fig. 2 shows the SEM images of the cross sections of the SPSed Ce^{3+}:$(Gd,Lu)_3Al_5O_{12}$ compacts after annealing. All specimens were densified at the final sintering temperature of

1250°C. However, the microstructures for the two SPS profiles differed in terms of grain size, pore size, and porosity. The microstructural parameters (grain size, pore size, and porosity) calculated from the SEM images are summarized in Table 2. Applying the two-step profile made it possible to significantly lower the porosity at the same sintering temperature. All two-step SPSed specimens showed lower porosity than that of the single-step SPSed specimen (SS-1250) (3.74%). In particular, the TS-1000 exhibited a porosity of 1.63%, indicating that a significant reduction in porosity was possible by applying the two-step SPS profile. The significant decrease in the porosity of the two-step SPSed specimens was due to improvement in their shrinkage behavior, i.e., fewer residual pores and a lower shrinkage-completion temperature, as shown in Fig. 2. In addition, as the first step temperature in the two-step profile was reduced, the grain size decreased gradually from 207 to 139 nm, and the pore size decreased from 72 to 43 nm. This microstructural change was due to the microstructure control of the two-step profile [18,19]. In this study, microstructure control using the two-step profile was expected to improve the optical properties as well.

3.2. Optical appearance and transmittance

The optical appearances of the Ce^{3+}:$(Gd,Lu)_3Al_5O_{12}$ compacts after annealing are shown in Fig. 3. The optical appearances and transparency of the annealed specimens placed on the grid can be easily compared. SS-1250 exhibited the lowest optical transparency among all specimens. Applying the modified two-step profile improved the optical appearance of the compacts. For two-step SPSed specimens, the optical appearance improved with a decrease in the heating rate at the second step. However, the most significant improvement was observed at the first step temperature of 1000°C. This indicates that a decrease in the heating

rate at the critical temperature for densification had a more significant effect than simply reducing the heating rate to improve the optical appearance. Therefore, at the first step temperature of 1000°C, porosity was lowest and the optical appearance also improved the most. The microstructure and optical appearance analysis results indicate that the TS-1000 specimen showed the highest transmittance among all specimens investigated in the present work.

Fig. 4 shows the in-line transmittance (ILT) curves of the sintered Ce^{3+}:$(Gd,Lu)_3Al_5O_{12}$ compacts after annealing. Significant light absorption was in the range of 420–500 nm. According to the reported results [27], well-fabricated $Lu_{2.7}Gd_{0.3}Al$-O_{12} ceramics exhibited excellent transmittance above 250 nm. In the present work, since light absorption by Ce^{3+} occurred at less than 500 nm, transmittance decreased rapidly. Owing to the light absorption due to the $4f \rightarrow 5d_2$ and $4f \rightarrow 5d_1$ transitions of Ce^{3+} at 340 nm and over a wavelength range of 420–500 nm, respectively, a strong light absorption band was detected [28]. The optical transmittance of the specimens showed the same trend as that of their optical appearance. At the same sintering temperature of 1250°C, all two-step SPSed specimens showed improved transmittance as compared to the single-step SPSed specimen. The TS-1000 specimen showed the most improved ILT of 56.5% at 1000 nm as compared to that (50.1%) of the SS-1250 specimen. In transparent ceramics, the area of the grain boundary also affects transmittance; however, porosity is the most critical factor [29]. In the case of the TS-1000 specimen, the first step temperature was 1000°C, at which shrinkage began, and porosity decreased significantly from 3.74% (SS-1250) to 1.63% (TS-1000). This decrease in porosity had a significant effect on the transmittance of the ceramic. In addition, as can be observed from Table 2, the porosity of the specimens showed a trend similar to that shown by the

optical transmittance. The TS-1000 specimen showed slightly reduced grain and pore sizes and significantly reduced porosity as compared to the SS-1250 specimen. The decrease in porosity, which had the most critical effect on transmittance, resulted in the most noticeable improvement in the transmittance of the TS-1000 specimen. $(Gd,Lu)_3Al_5O_{12}$:Ce ceramics with a composition similar to that of the ceramics prepared in this study were fabricated by conventional sintering at 1750°C for 4 h under a vacuum atmosphere after cold isostatic press at 240 MPa [14]. As a result, an ILT of approximately 72% was achieved at 1000 nm, showing excellent optical properties. Although there have been reports of preparing garnet materials with full densification and high transmittance by conventional sintering, it is difficult to achieve high transmittance with the SPS method. In a previous study, Nd:YAG ceramics were fabricated using the reactive-SPS method by applying a two-step heating profile [30]. The Nd:YAG powder was heated at 100°C/min to the first step temperature of 1000°C with an applied pressure of 70 MPa and at 15°C/min to the second step temperature of 1350°C, which was maintained for 5 min. However, an ILT of approximately 36% was obtained at 1000 nm, and excellent optical properties were not achieved. In this study, although the ILT was not close to the theoretical value, the transmittance could be improved through the application of the two-step profile and microstructure control.

3.3. Oxidation state and PL characteristic

XPS measurements were conducted to investigate the oxidation states of the Ce dopant, and the results of the powder, single-step profile (SS-1250), and two-step profile (TS-1000) are summarized in Fig. 5. The red lines represent the spectra of Ce^{3+} ions and the blue lines represent the spectra of Ce^{4+} ions. The fractions of the Ce^{3+} and Ce^{4+} ions were calculated

from the areas of their spectra. For comparing the as-synthesized powder with the compacts sintered in the single-step and two-step profiles, the fraction of Ce^{3+} in the as-synthesized powder was required. The fraction of Ce^{3+} in the powder was 61.42%, as shown in Fig. 5 (a). The Ce^{3+} fraction of the SS-1250 specimen was 61.73%, which is almost the same as that of the synthesized powder. However, because of slight oxidation, the TS-1000 specimen showed a Ce^{3+} fraction of 60.66%. As the SPS process provides an oxidizing atmosphere of graphite components, oxidation occurred in the two-step profile with a long sintering time, and the fraction of Ce^{3+} decreased slightly. The slightly decreased Ce^{3+} fraction of the two-step profile affected its PL characteristics along with the microstructure.

Fig. 6 (a) shows the PL excitation spectra of the Ce^{3+}:$(Gd,Lu)_3Al_5O_{12}$ compacts after annealing. PL excitation measurements were performed to investigate the wavelength-dependent excitation when 571 nm light was emitted. Excitation bands were detected at approximately 342, 453, and 506 nm, corresponding to the excitation of Ce^{3+} [31,32]. The excitation peak at approximately 342 nm correspond to the transition of Ce^{3+} from the ground state ($2F_{5/2}$) to the T_{2g} state. Excitation peaks at approximately 453 and 506 nm corresponded to the transition from the ground state to the E_{2g} state [31,32]. The SS-1250 specimen exhibited significantly higher PL excitation intensity than did the two-step profile specimens. Independent of the first step temperature, the PL excitation of the TS-1000 specimen intensity was the lowest. Their porosity strongly influenced the transmittance of the specimen, and the two-step profile showed better results than did the single-step profile. However, the PL excitation characteristics showed an opposite trend. First, the fraction of Ce^{3+} (Fig. 5) directly affected the PL excitation characteristics of the specimens. Because the PL excitation was caused only by Ce^{3+} [31,32], the fraction of Ce^{3+} present in the Ce^{3+}:$(Gd,Lu)_3Al_5O_{12}$ ceramics

was a very important factor. Next, the grain size of the SS-1250 specimen was the largest at 221 nm, which decreased gradually from 207 to 139 nm with a decrease in the first step temperature. Owing to its large grain size and small grain boundary area, the single-step profile affected the PL excitation characteristics of the compacts more than the two-step profile did [33,34]. Fig. 6 (b) shows the PL emission spectra of the Ce^{3+}:$(Gd,Lu)_3Al_5O_{12}$ compacts after annealing. The wavelength-dependent emission of the compacts under excitation by a wavelength of 453 nm was investigated. The PL emission characteristics of the compacts showed the same trend as that shown by the PL excitation characteristics. The full widths at half maximum values were almost the same for all specimens. This indicates that the crystallinity and light clarity of all specimens were almost the same and that the two-step profile did not affect the PL emission characteristics.

4. Conclusions

In this study, a two-step SPS profile was employed to improve the optical properties of Ce^{3+}:$(Gd,Lu)_3Al_5O_{12}$ ceramics as attractive yellow-emitting phosphors. The shrinkage curve of the two-step profile showed a significant reduction in porosity from 3.74% to 1.63% at the first step temperature of 1000°C, at which shrinkage began. As the first step temperature decreased, the microstructure control of the two-step profile refined the microstructure of the compacts by reducing the grain and pore sizes. As a result of the significant reduction in porosity in the two-step profile, transmittance improved from 50.1% to 56.5% at 1000 nm. On the other hand, oxidation occurred owing to the two-step profile's long sintering time, and the fraction of Ce^{3+} decreased slightly. Therefore, the two-step profile did not affect the ceramics' PL excitation and emission characteristics.

Acknowledgments

I would like to thank Dr. Craig A.J. Fisher of Japan Fine Ceramics Center (JFCC) for his constructive discussion on arranging and interpreting the transmittance and XPS results.

References

[1] J.G. Li, Y. Sakka, Recent progress in advanced optical materials based on gadolinium aluminate garnet ($Gd_3Al_5O_{12}$), Sci. Technol. Adv. Mater. 16 (2015) 014902.

[2] M. Wang, B. Lu, Manufacture and Faraday magneto-optical effect of highly transparent novel holmium aluminum garnet ceramics, Scripta Mater. 195 (2021) 133729.

[3] I. Milisavljevic, G. Zhang, Y. Wu, Solid-state single-crystal growth of YAG and Nd: YAG by spark plasma sintering, J. Mater. Sci. Technol. 106 (2022) 118–127.

[4] C. Kim, W. Lee, A. Melis, A. Elmughrabi, K. Lee, C. Park, J.Y. Yeom, A Review of Inorganic Scintillation Crystals for Extreme Environments, Crystals 11 (2021) 669.

[5] V. Balaram, Rare earth elements: A review of applications, occurrence, exploration, analysis, recycling, and environmental impact, Geosci. Front. 10 (2019) 1285–1303.

[6] T. Shishido, K. Okamura, S. Yajima, $Gd_3Al_5O_{12}$ Phase Obtained by Crystallization of Amorphous $Gd_2O_3 \cdot 5/3Al_2O_3$, J. Am. Ceram. Soc. 61 (1978) 373–375.

[7] J. Li, J.G. Li, S. Liu, X. Li, X. Sun, Y. Sakka, The development of Ce^{3+}-activated $(Gd,Lu)_3Al_5O_{12}$ garnet solid solutions as efficient yellow-emitting phosphors, Sci. Technol. Adv. Mater. 14 (2013) 054201.

[8] B.N. Kim, K. Morita, T.S. Suzuki, J.G. Li, H. Matsubara, Simulation of densification behavior of nano-powder in final sintering stage: Effect of pore-size distribution, J. Eur. Ceram. Soc. 41 (2021) 625–634.

[9] M. Tokita, Progress of Spark Plasma Sintering (SPS) Method, Systems, Ceramics Applications and Industrialization, Ceramics 4 (2021) 160–198.

[10] A. Wagner, Y. Meshorer, B. Ratzker, D. Sinefeld, S. Kalabukhov, S. Goldring, E.

Galun, N. Frage, Pressure‐assisted sintering and characterization of Nd:YAG ceramic lasers, Sci. Rep. 11 (2021) 1512.

[11] A. Wagner, B. Ratzker, S. Kalabukhov, S. Kolusheva, M. Sokol, N. Frage, Highly-doped Nd:YAG ceramics fabricated by conventional and high pressure SPS, Ceram. Int. 45 (2019) 12279–12284.

[12] S.F. Wang, J. Zhang, D.W. Luo, F. Gu, D.Y. Tang, Z.L. Dong, G.E.B. Tan, W.X. Que, T.S. Zhang, S. Li, L.B. Kong, Transparent ceramics: Processing, materials and applications, Prog. Solid. State. Chem. 41 (2013) 20–54.

[13] J.H. Lee, J.G. Li, B.N. Kim, Q. Meng, X. Sun, B.K. Jang, Effect of annealing on microstructure and luminescence characteristics in spark plasma sintered Ce^{3+}-activated $(Gd,Lu)_3Al_5O_{12}$ garnet ceramics, J. Eur. Ceram. Soc. 41 (2021) 1586–1592.

[14] Z. Sun, Z. Chen, M. Wang, B. Lu, Production and optical properties of Ce^{3+}-activated and Lu^{3+}-stabilized transparent gadolinium aluminate garnet ceramics, J. Am. Ceram. Soc. 103 (2020) 809–818.

[15] X. Chen, X. Liu, Y. Feng, X. Li, H. Chen, T. Xie, H. Kou, R. Kucerkova, Microstructure evolution in two-step-sintering process toward transparent Ce:$(Y,Gd)_3(Ga,Al)_5O_{12}$ scintillation ceramics. J. Alloys Compd. 846 (2020) 156377.

[16] J. Li, Q. Chen, G. Feng, W. Wu, D. Xiao, J. Zhu, Optical properties of the polycrystalline transparent Nd:YAG ceramics prepared by two-step sintering, Ceram. Int. 38S (2012) S649–S652.

[17] Z. Seeley, N. Cherepy, S. Payne, Two-step sintering of $Gd_{0.3}Lu_{1.6}Eu_{0.1}O_3$ transparent ceramic scintillator, Opt. Mater. Express. 3 (2013) 908–912.

[18] W.K. Jung, H.J. Ma, D.G. Kim, D.K. Kim, Two-step sintering behavior of titanium-

doped Y_2O_3 ceramics with monodispersed sub-micrometer powder, Ceram. Int. 45 (2019) 510–515.

[19] H.J. Ma, W.K. Jung, C. Baek, D.K. Kim, Influence of microstructure control on optical and mechanical properties of infrared transparent Y_2O_3-MgO nanocomposite, J. Eur. Ceram. Soc. 37 (2017) 4902–4911.

[20] H. Furuse, S. Nakasawa, H. Yoshida, K. Morita, T.S. Suzuki, B.N. Kim, Y. Sakka, K. Hiraga, Transparent ultrafine Yb^{3+}:Y_2O_3 laser ceramics fabricated by spark plasma sintering, J. Am. Ceram. Soc. 101 (2018) 694–702.

[21] K. Morita, B.N. Kim, H. Yoshida, H. Zhang, K. Hiraga, Y. Sakka, Effect of loading schedule on densification of $MgAl_2O_4$ spinel during spark plasma sintering (SPS) processing, J. Eur. Ceram. Soc. 32 (2012) 2303–2309.

[22] M. Nanko, K.Q. Dan, Two-step pulsed electric current sintering of transparent Al_2O_3 ceramics, Adv. Appl. Ceram. 113 (2014) 80–84.

[23] H.H. Nguyen, M. Nanko, Densification and grain growth of large-sized polycrystalline Al_2O_3 during a two-step pulsed electric current sintering process, Mater. Trans. 59 (2018) 1610–1615.

[24] J.H. Lee, B.N. Kim, B.K. Jang, Fabrication of transparent Y_2O_3 ceramics by two-step spark plasma sintering, J. Am. Ceram. Soc. 104 (2021) 5501–5508.

[25] J. Li, J.G. Li, X. Li, X. Sun, Photoluminescence properties of phosphors based on Lu^{3+}-stabilized $Gd_3Al_5O_{12}$:Tb^{3+}/Ce^{3+} garnet solid solutions, Opt. Mater. 62 (2016) 328–334.

[26] S. Grasso, C. Hu, G. Maizza, B.N. Kim, Y. Sakka, Effects of pressure application method on transparency of spark plasma sintered alumina, J. Am. Ceram. Soc. 94 (2011) 1405–1409.

[27] P. Ma, T. Xie, L. Wu, H. Chen, H. Kou, Y. Shi, Y. Pan, J. Li, Fabrication of Nd:$Lu_{2.7}Gd_{0.3}Al_5O_{12}$ transparent ceramics by solid-state reactive sintering, Opt. Mater. 66 (2017) 422–427.

[28] S. Feng, H. Qin, G. Wu, H. Jiang, J. Zhao, Y. Liu, Z. Luo, J. Qioa, J. Jiang, Spectrum regulation of YAG:Ce transparent ceramics with Pr, Cr doping for white light emitting diodes application, J. Eur. Ceram. Soc. 37 (2017) 3403–3409.

[29] T. Benitez, S.Y. Gomez, A. Oliveira, N. Travitzky, D. Hotza, Transparent ceramic and glass-ceramic materials for armor applications, Ceram. Int. 43 (2017) 13031–13046.

[30] D.Y. Kosyanov, A.A. Vornovskikh, A.M. Zakharenko, E.A. Gridasova, R.P. Yavetskiy, M.V. Dobrotvorskaya, A.V. Tolmachev, O.O. Shichalin, E.K. Papynov, A.Y. Ustinov, V.G. Kuryavyi, A.A. Leonov, S.A. Tikhonov, Influence of sintering parameters on transparency of reactive SPSed Nd^{3+}:YAG ceramics, Opt. Mater. 112 (2021) 110760.

[31] X. Su, K. Zhang, Q. Liu, H. Zhong, Y. Shi, Y. Pan, Combinatorial Optimization of $(Lu_{1-x}Gd_x)_3Al_5O_{12}$:$Ce_{3y}$ Yellow Phosphors as Precursors for Ceramic Scintillators, ACS Comb. Sci. 13 (2011) 79–83.

[32] A. Birkel, K.A. Denault, N.C. George, C.E. Doll, B. Hery, A.A. Mikhailovsky, C.S. Birkel, B.C. Hong, R. Seshadri, Rapid Microwave Preparation of Highly Efficient Ce^{3+}-Substituted Garnet Phosphors for Solid State White Lighting, Chem. Mater. 24 (2012) 1198–1204.

[33] B. Wen, D.F. Zhang, N. Zhang, J.K. Feng, B. Jiang, F.S. Pan, Y. Zhang, L. Yang, Effect of grain size on the luminescent properties of Ce^{3+} doped $Y_3Al_5O_{12}$ ceramic phosphor plates, Ceram. Int. 46 (2020) 10452–10456.

[34] Y. Kim, S. Jang, Effect of particle size on photoluminescence emission intensity of

ZnO, Acta Mater. 59 (2011) 3024–3031.

Figure captions

Figure 1. SPS curves of the SPSed Ce^{3+}:$(Gd,Lu)_3Al_5O_{12}$ ceramics (a) single-step SPS (SS-1250) and (b) two-step SPS (TS-1000).

Figure 2. SEM images of the cross sections of the SPSed Ce^{3+}:$(Gd,Lu)_3Al_5O_{12}$ ceramics.

Figure 3. Optical appearances of the SPSed Ce^{3+}:$(Gd,Lu)_3Al_5O_{12}$ ceramics under the conditions listed in Table 1.

Figure 4. (a) Transmittance curves of the SPSed Ce^{3+}:$(Gd,Lu)_3Al_5O_{12}$ ceramics after annealing; (b) the curve magnified over the wavelength of 750–1050 nm.

Figure 5. XPS profiles of the (a) Ce^{3+}:$(Gd,Lu)_3Al_5O_{12}$ powder, (b) single-step SPSed compact (SS-1250), and (c) two-step SPSed compact (TS-1000).

Figure 6. (a) PL excitation and (b) PL emission spectra of Ce^{3+}:$(Gd,Lu)_3Al_5O_{12}$ ceramics with different SPS conditions after annealing.

Figures

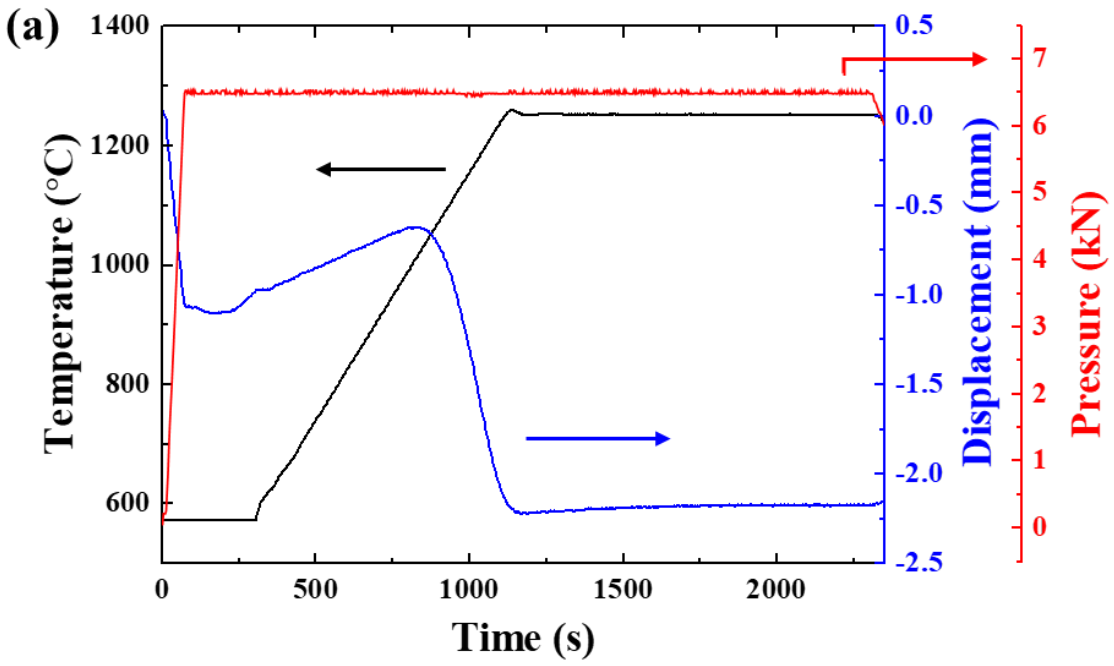

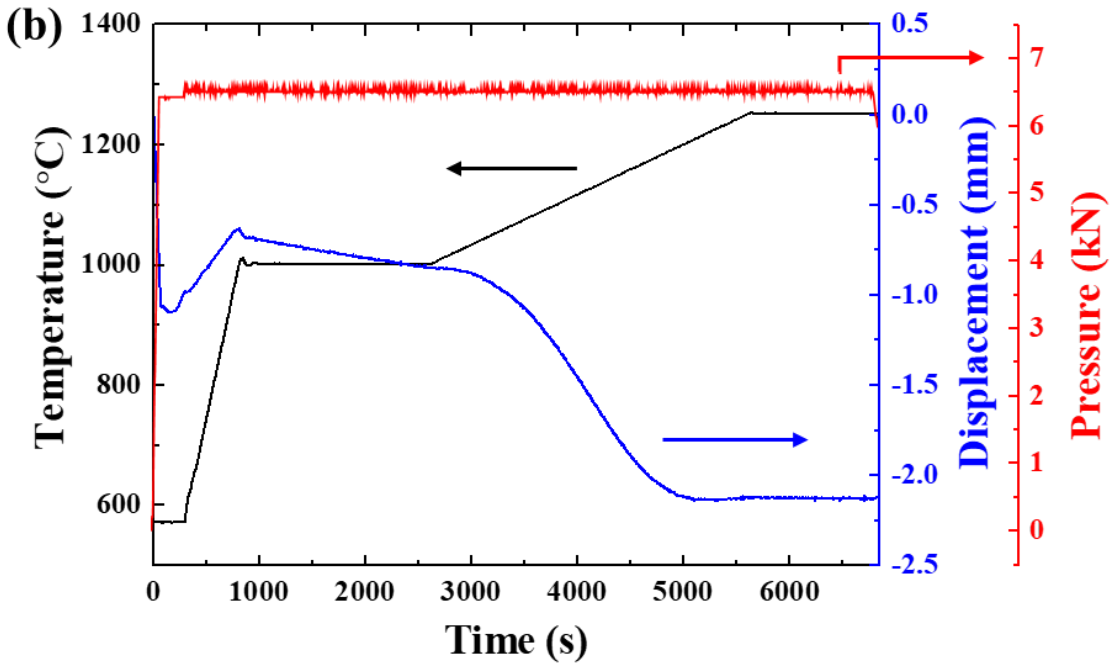

Fig. 1

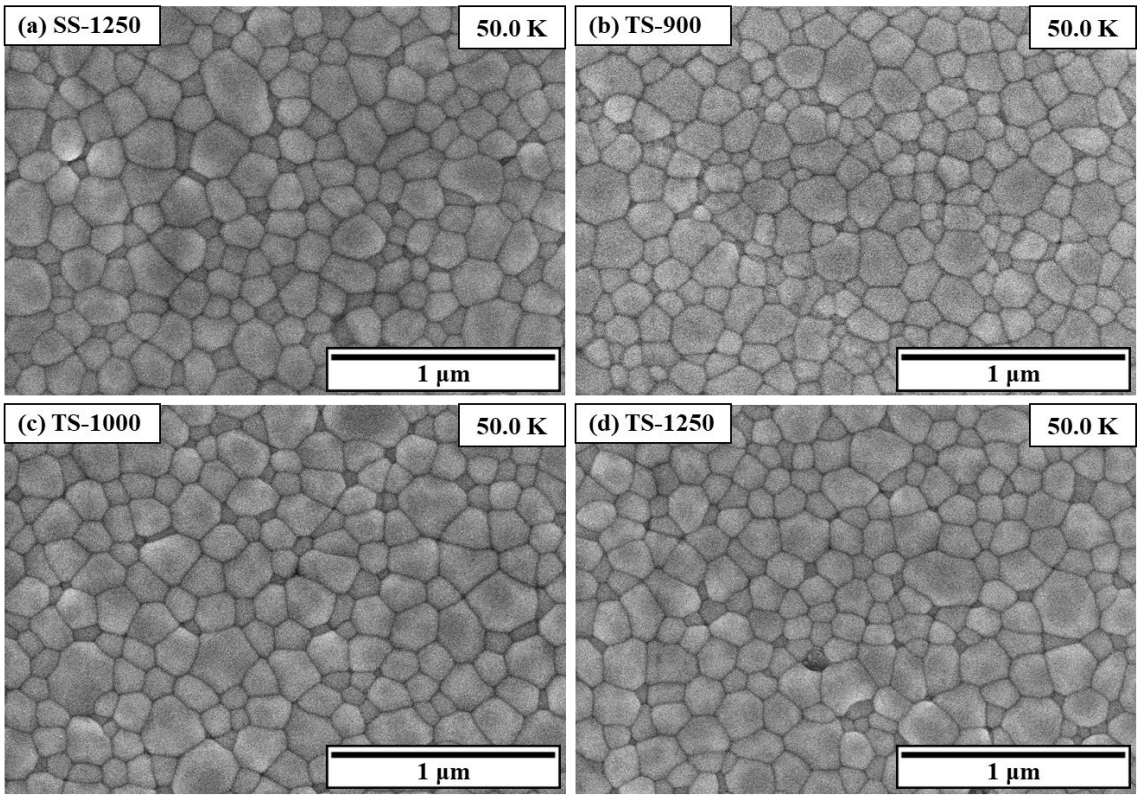
(a) SS-1250
50.0 K
1 µm
(b) TS-900
50.0 K
1 µm
(c) TS-1000
50.0 K
1 µm
(d) TS-1250
50.0 K
1 µm

Fig. 2

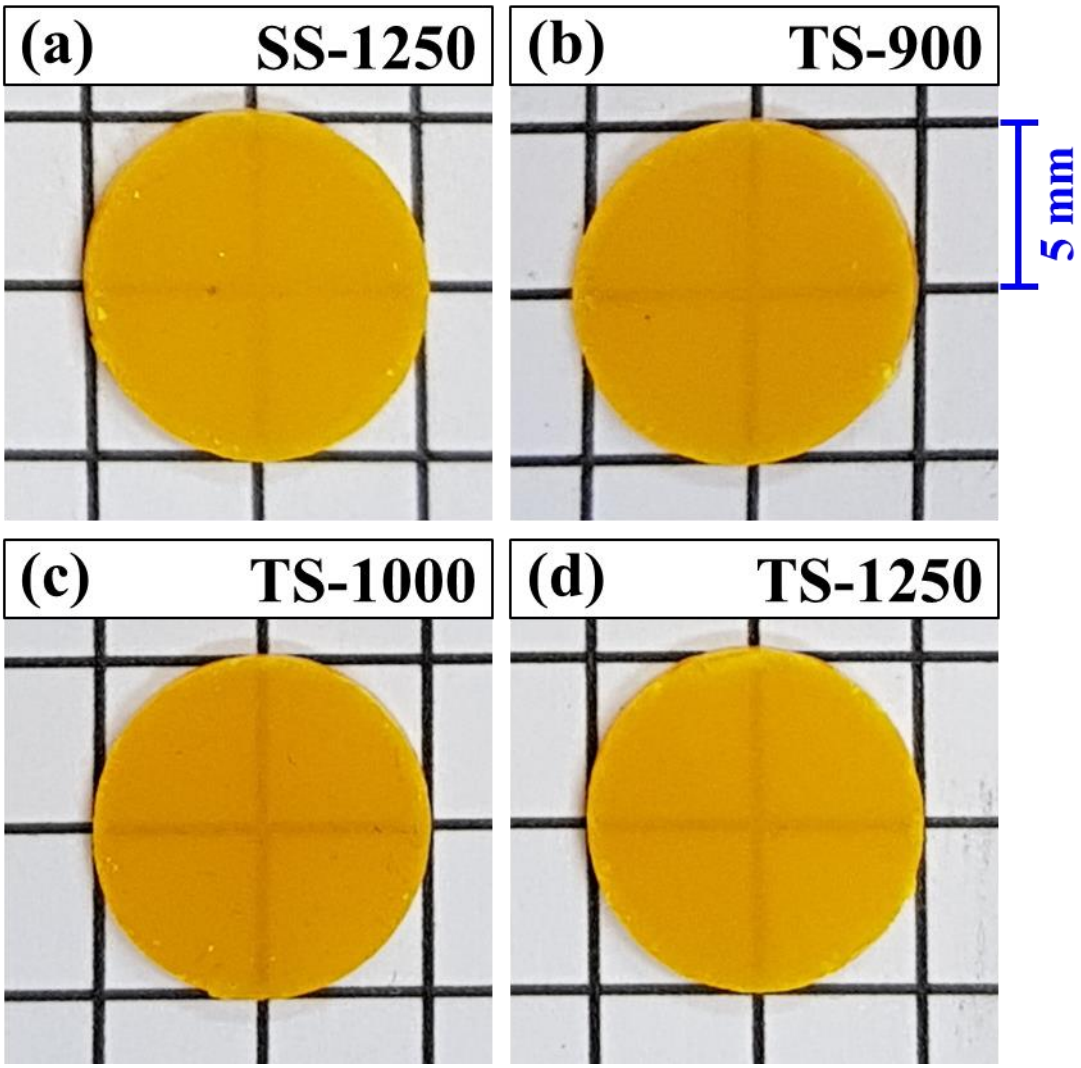

Fig. 3

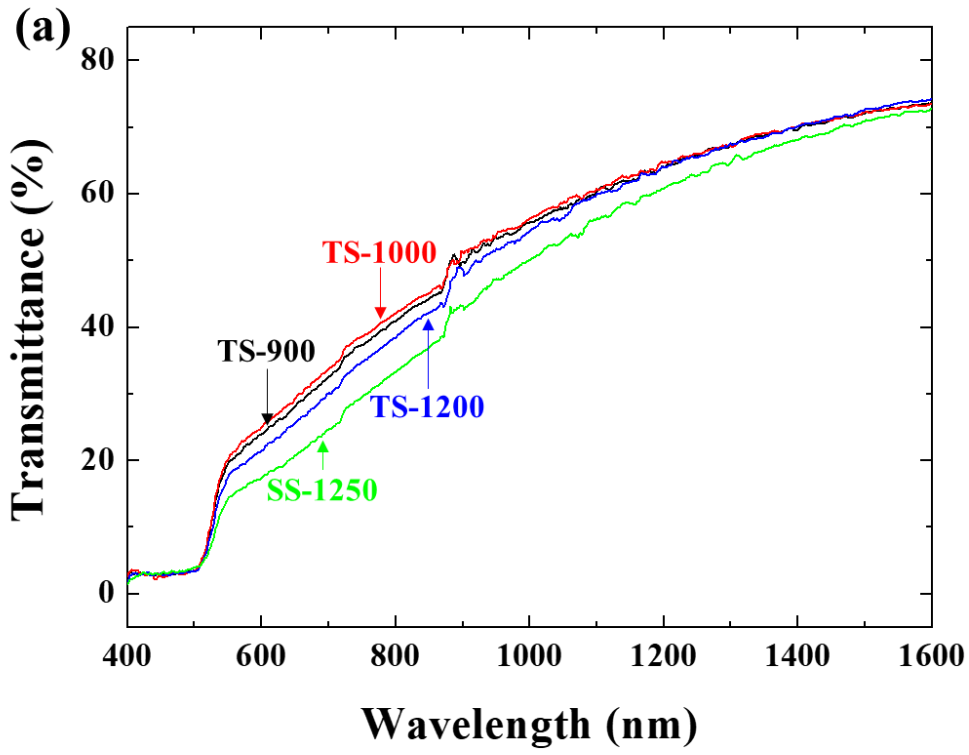
(a)
Transmittance (%)
Wavelength (nm)
TS-1000
TS-900
TS-1200
SS-1250
0
20
40
60
80
400
600
800
1000
1200
1400
1600

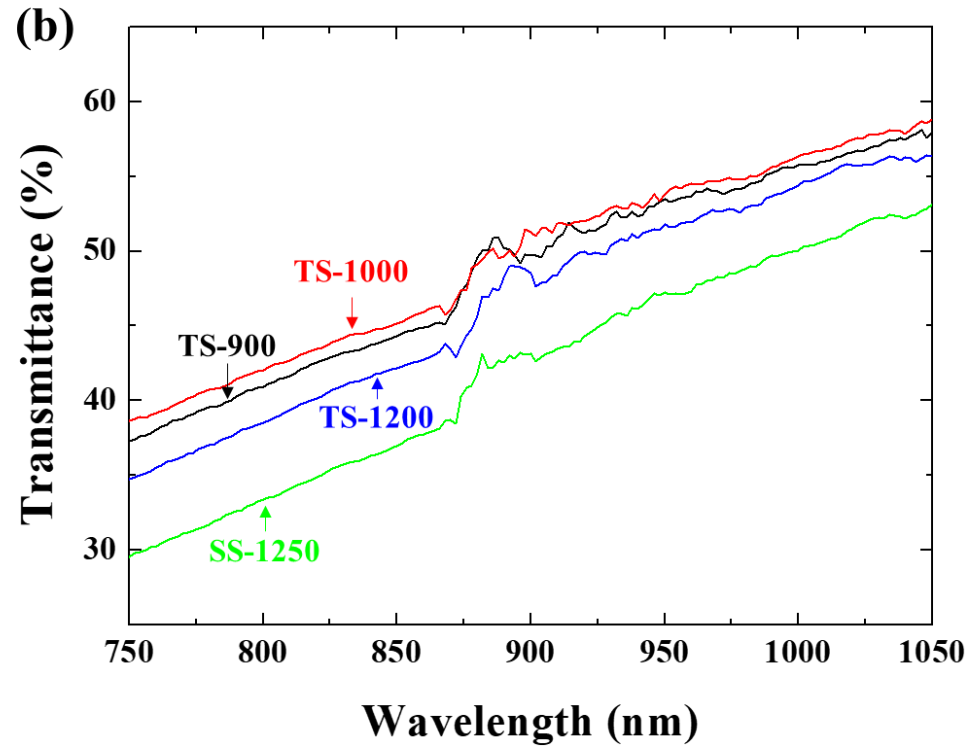
(b)
Transmittance (%)
Wavelength (nm)
TS-1000
TS-900
TS-1200
SS-1250
30
40
50
60
750
800
850
900
950
1000
1050

Fig. 4

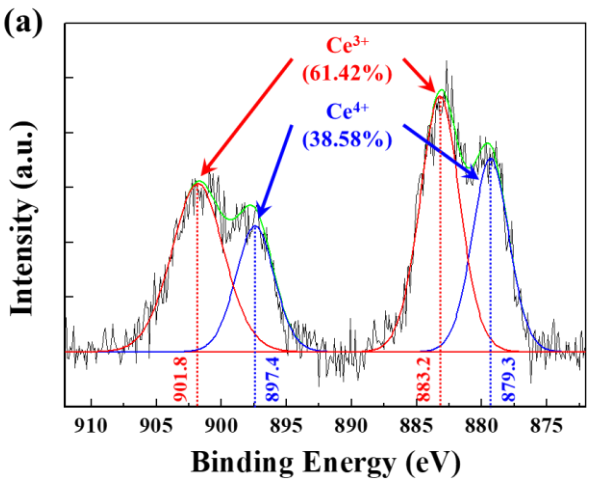
(a)
Ce3+
(61.42%)
Ce4+
(38.58%)
Intensity (a.u.)
901.8
897.4
883.2
879.3
910 905 900 895 890 885 880 875
Binding Energy (eV)

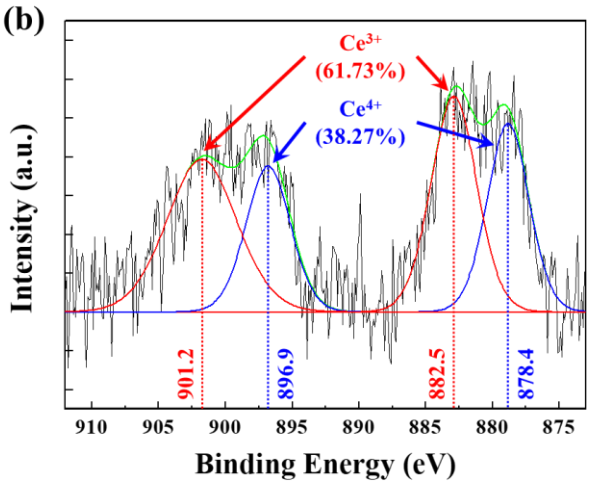
(b)
Ce3+
(61.73%)
Ce4+
(38.27%)
Intensity (a.u.)
901.2
896.9
882.5
878.4
910 905 900 895 890 885 880 875
Binding Energy (eV)

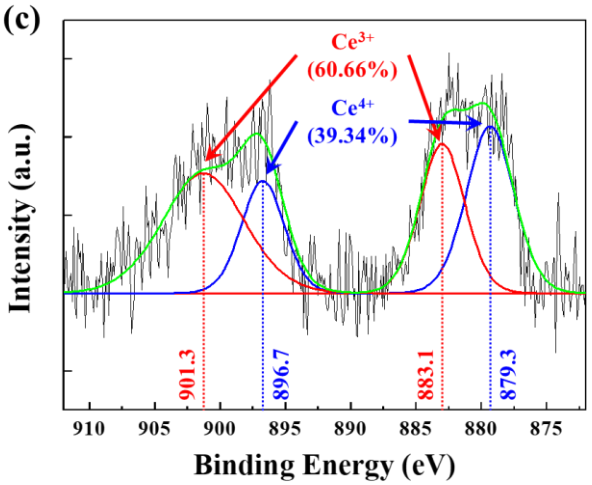
(c)
Ce3+
(60.66%)
Ce4+
(39.34%)
Intensity (a.u.)
901.3
896.7
883.1
879.3
910 905 900 895 890 885 880 875
Binding Energy (eV)

Fig. 5

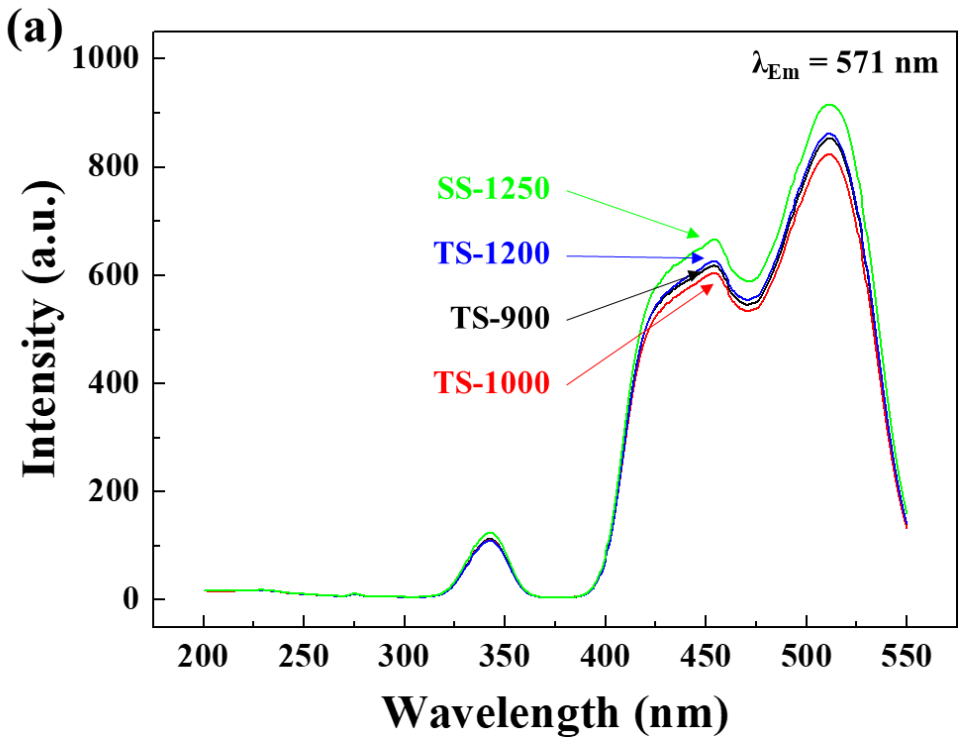
(a)
λEm = 571 nm
SS-1250
TS-1200
TS-900
TS-1000
Intensity (a.u.)
Wavelength (nm)
0
200
400
600
800
1000
200
250
300
350
400
450
500
550

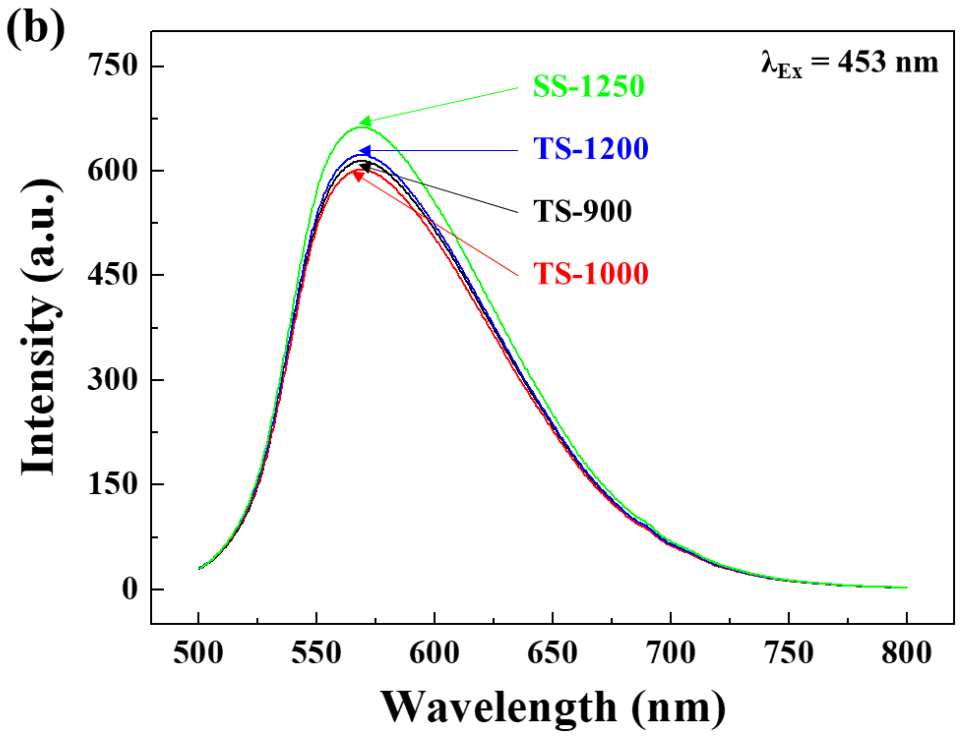
(b)
λEx = 453 nm
SS-1250
TS-1200
TS-900
TS-1000
Intensity (a.u.)
Wavelength (nm)
0
150
300
450
600
750
500
550
600
650
700
750
800

Fig. 6

Tables

Table 1. SPS conditions of Ce^{3+}:$(Gd,Lu)_3Al_5O_{12}$ ceramics.

No.	Specimen name	SPS profile		Heating rate	Range (°C)	Holding stage
1	SS-1250	Single-step profile		50°C/min	600–1250	@ 1250°C for 20 min
2	TS-900	Two-step profile	1st step	50°C/min	600–900	@ 900°C for 30 min
			2nd step	5°C/min	900–1250	@ 1250°C for 20 min
3	TS-1000		1st step	50°C/min	600–1000	@ 1000°C for 30 min
			2nd step	5°C/min	1000–1250	@ 1250°C for 20 min
4	TS-1200		1st step	50°C/min	600–1200	@ 1200°C for 30 min
			2nd step	5°C/min	1200–1250	@ 1250°C for 20 min

Table 2. Microstructure parameters of SPSed Ce^{3+}:$(Gd,Lu)_3Al_5O_{12}$ ceramics.

No.	Specimen name	Grain size	Pore size	Porosity
1	SS-1250	221 nm	81 nm	3.74%
2	TS-900	139 nm	43 nm	2.29%
3	TS-1000	163 nm	69 nm	1.63%
4	TS-1200	207 nm	72 nm	2.96%

Declaration of interests

☒ The authors declare that they have no known competing financial interests or personal relationships that could have appeared to influence the work reported in this paper.

☐The authors declare the following financial interests/personal relationships which may be considered as potential competing interests: